Xie *et al. Energy Mater* 2022;2:200008
DOI: 10.20517/energymater.2022.04

Energy Materials

Review

Open Access

Check for updates

Two-dimensional nanofluidics for blue energy harvesting

Linhan Xie#, Jiadong Tang#, Runan Qin, Jingbing Liu, Qianqian Zhang*, Yuhong Jin, Hao Wang*

Key Laboratory for New Functional Materials of Ministry of Education, Faculty of Materials and Manufacturing, Beijing University of Technology, Beijing 100124, China.

***Correspondence to:** Prof./Dr. Qianqian Zhang, Key Laboratory for New Functional Materials of Ministry of Education, Faculty of Materials and Manufacturing, Beijing University of Technology, No. 100 Pingleyuan, Chaoyang District, Beijing 100124, China. E-mail: zhangqianqian@bjut.edu.cn; Prof./Dr. Hao Wang, Key Laboratory for New Functional Materials of Ministry of Education, Faculty of Materials and Manufacturing, Beijing University of Technology, No. 100 Pingleyuan, Chaoyang District, Beijing 100124, China. E-mail: haowang@bjut.edu.cn

How to cite this article: Xie L, Tang J, Qin R, Liu J, Zhang Q, Jin Y, Wang H. Two-dimensional nanofluidics for blue energy harvesting. *Energy Mater* 2022;2:200008. https://dx.doi.org/10.20517/energymater.2022.04

Received: 26 Jan 2022 **First Decision:** 26 Feb 2022 **Revised:** 10 Mar 2022 **Accepted:** 15 Mar 2022 **Published:** 31 Mar 2022

Academic Editors: Yuping Wu, Hong Xu **Copy Editor:** Xi-Jun Chen **Production Editor:** Xi-Jun Chen

Abstract

Blue energy harvesting based on the ion flow obtained from seas and rivers provides a clean, stable and continuous electric output that is highly dependent on ion-selective membranes (ISMs) that conduct single ions. In recent years, ISMs constructed based on two-dimensional (2D) nanofluidics have demonstrated promising application prospects in blue energy harvesting due to their facile fabrication, excellent ion selectivity and high ion flux. In this review, the principles of 2D nanofluidics in regulating ionic transport are firstly proposed and discussed, including ion selectivity and ultrafast ion transmission, which are considered as two critical factors for achieving highly efficient blue energy harvesting. The advantages of 2D nanofluidics towards blue energy harvesting are analyzed to reveal the necessity of this review. The construction of 2D nanofluidic membranes based on several typical materials and their recent research advances in salinity gradient- and pressure-driven blue energy harvesting are also summarized in detail. Finally, the existing challenges of 2D nanofluidic membranes regarding blue energy harvesting applications are discussed to provide new insights for the development of high-performance blue energy harvesting systems based on 2D nanofluidics.

Keywords: Blue energy harvesting, 2D nanofluidics, ion flow, osmotic energy, pressure-driven power generation

INTRODUCTION

Ocean energy, also known as blue energy, is considered as a promising alternative to traditional fossil fuels, owing to its ideal environmental friendliness and large reserves[1-3]. The blue energy stored in the oceans comes in various forms, including tidal, wave, temperature difference and osmotic energies[4,5]. However, most blue energy, such as tidal energy, suffers from an intermittent power supply caused by environmental and climate changes, which limits its real-world applications in stable electric supplies. Thus, it is a challenge to harvest blue energy in a continuous and stable output manner. In comparison, the blue energy based on directed ion flow (i.e., ion current) is minimally affected by environmental changes, which could provide a relatively stable and sustainable electric output for all weather and time conditions. The driving force of a directed ion current involves a salinity gradient and pressure difference. For instance, the salinity gradient between a sea and river or two different seawaters can produce considerable electric power, i.e., osmotic energy[6]. The energy produced by the mixing of river and seawater is estimated to be 0.8 kWh m^{-3}, which is ~8% of the energy produced by burning natural gas at the same mass[7-9]. On this basis, there are 1.4-2.6 TW h of power generation per year when the osmotic energy from the oceans of the Earth is fully utilized, thereby potentially reducing our dependence on fossil fuels[10]. Hence, ion flow represents a promising method for the development of efficient blue energy harvesting.

Power generation from ion flow is highly dependent on ion-selective membranes (ISMs) that conduct single ions (cations or anions). Under a driving force, the single ions flow through the ISMs to generate a transmembrane electrochemical potential gradient, which can be directly converted into electrical energy output to an external circuit[11-13]. Traditional ISMs are usually polymer membranes, such as Nafion, although their low ion flux limits the energy conversion efficiency. In recent years, the emerging nanofluidic technology has provided new insights into the development of ideal ISMs with excellent ion selectivity and high ion flux. Nanofluidic membranes are inspired by biological cell membranes with embedded ion channels, which have plentiful nanoscale channels with excess charge on their interior surfaces[14,15]. The strong electrostatic field in the nanoconfined space contributes to outstanding ion selectivity[16]. The nanoconfined space of nanofluidic membranes also helps to realize the effective and rapid sieving of different ions, which is of great significance for many environmental and energy fields[17-19]. In addition, nanofluidic membranes have excellent mass transfer performance, with the mass transfer rate of water molecules equivalent to that of carbon nanotubes[20]. Combined with their excellent ion selectivity, nanofluidic membranes can be widely used in the construction of concentration cells and pressure-driven power generators, demonstrating significant application potential for blue energy harvesting[21-23].

Nanofluidics can be categorized according to their different ion transport paths [Figure 1], namely, one-dimensional (1D) nanofluidics, two-dimensional (2D) nanofluidics (i.e., layered membranes) and three-dimensional (3D) nanofluidics (i.e., porous membranes)[24]. 1D and 3D nanofluidic materials, such as polymers, are difficult to fabricate and costly to carve holes[25,26]. In comparison, 2D nanofluidics with horizontal and vertical directions for ion transport have attracted significant interest in recent years because of their simple preparation process and facile modifications compared with their 1D and 3D counterparts[27]. Some typical 2D materials, such as graphene oxide (GO), montmorillonite (MMT), covalent organic frameworks (COFs) and transition metal carbides, carbonitrides and nitrides (MXenes), have been widely used to construct 2D nanofluidics for osmotic energy harvesting and deliver high power output density, owing to their excellent ion selectivity, high ion flux and ultrafast ion transport[28-32]. Thus, a comprehensive understanding of 2D nanofluidics is necessary for achieving highly efficient blue energy harvesting for real-world applications.

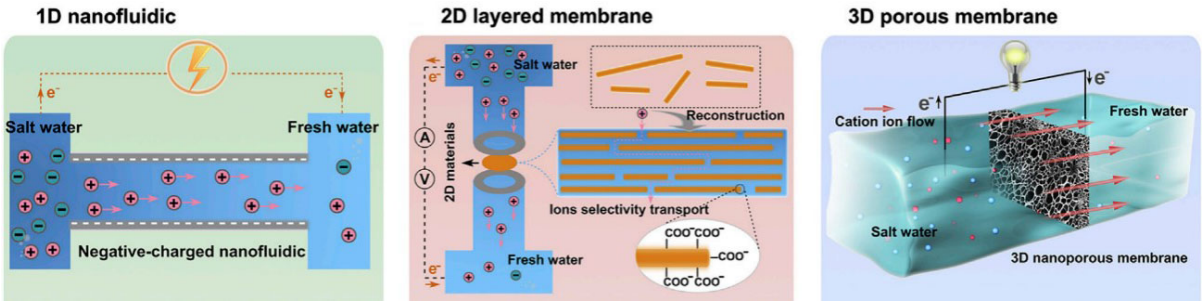

Figure 1. Classification of nanofluidics. Figure reproduced with permission from Xiao *et al.*[24] (Copyright © 2019 Elsevier).

In recent years, several impactful reviews concerning 2D nanofluidics have been published. For example, Liu *et al.*[33] summarized the synthesis strategies of the most widely used 2D materials and their applications in the field of separation. Gao *et al.*[34] discussed the characteristics of different 2D nanofluidics and their valuable applications in water treatment, energy storage and battery separators. However, a comprehensive discussion of 2D nanofluidics for regulating ion transport and harvesting blue energy is still lacking. In this review, the principles of ion transport regulated by 2D nanofluidics and recent advances in 2D nanofluidics towards blue energy harvesting are reviewed and discussed in detail. Firstly, the characteristics and advantages of 2D nanofluidics are introduced to demonstrate the necessity of their applications in blue energy harvesting. The construction of 2D nanofluidic membranes is then summarized and discussed in detail according to the various materials. Next, recent advances in 2D nanofluidics for blue energy harvesting are reviewed based on the two different driving forces of salinity gradient and pressure. Finally, the challenges and prospects of 2D nanofluidics are discussed to provide further directions for this field. It is anticipated that this review will provide a basis for the construction of high-performance 2D nanofluidics and the acquisition of high-efficiency blue energy.

FUNDAMENTALS OF 2D NANOFLUIDICS

Definition of 2D nanofluidics

Inspired by the nacreous layered microstructure and energy conversion in biological nanochannels, the materials design and application of artificial nanofluidic devices based on 2D fluid transport, i.e., 2D nanofluidics, have received extensive attention. The energy conversion systems of 2D nanofluidics imitate some aspects of energy conversion in biological systems in principle and structure and realize the conversion of different forms of energy through materials design and device assembly. 2D nanofluidics are usually constructed by the stacking of 2D nanosheets with atomic thickness. The assembled membranes then have lamellar spacing with nano or sub-nano height and form dense nanofluidic channels. The transmembrane ion transport through 2D nanofluidics can be divided into horizontal and vertical directions, as shown in Figure 2[35,36]. 2D nanofluidics have the characteristics of ion selective transport and ultrafast ion transport and show a wide range of applications in energy conversion and storage, molecular screening and water purification.

Advantages of 2D nanofluidics for blue energy harvesting

2D nanofluidics are characterized by their easy preparation, adjustable surface functionalization, excellent ion regulation ability, high ion flux and notable advantages in regulating ion transport[37-39].

Facile fabrication

The early research on nanofluidic systems was mostly focused on the design and preparation of 1D nanochannels. For example, Asghar *et al.*[40] fabricated 1D nanopores with diameters of several nm by

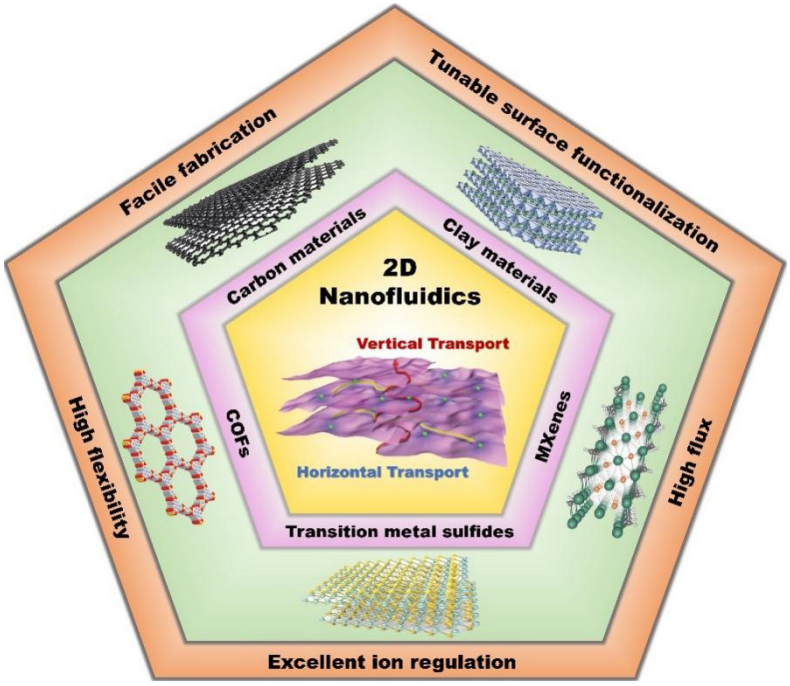

Figure 2. Fundamentals of 2D nanofluidics.

heating nanopores with diameters of 100 to 300 nm at high temperatures of > 1000 °C, followed by milling with a focused ion beam in free-standing membranes. Ho *et al.*[41] produced single synthetic nanometer-diameter pores using a tightly focused, high-energy electron beam to sputter atoms in 10-nm-thick silicon nitride membranes. Other complex fabrication techniques, such as heavy ion bombardment combined with chemical track etching, ion tracks in conjunction with deposition and so on, can also be used to fabricate 1D nanopores[42-44]. However, the techniques used to construct 1D nanofluidics are complex and expensive, which greatly limit the practical application of high-quality nanofluidics. In contrast, the self-assembly of 2D nanofluidic membranes is mediated by van der Waals interactions. The specific surface area of 2D nanomaterials with a high aspect ratio is large, which increases the interaction between layers and is conducive to the assembly of membranes. High-quality 2D nanofluidic membranes can be obtained by simple methods, such as vacuum filtration, interfacial polymerization and so on[45,46]. Therefore, 2D nanofluidics have the characteristics of easy preparation and low cost and therefore possess greater advantages in practical applications.

Tunable surface functionalization

Tunable surface functionalization is another important feature of 2D nanofluidics. The modification methods mainly include electrostatic self-assembly, covalent bond modification and fiber intercalation[47,48]. Electrostatic self-assembly is a technology that makes the basic structural units spontaneously form an ordered structure through the electrostatic force of non-chemical bonds without an external force. For example, Ding *et al.*[49] modified MXene nanosheets with polydiallyl dimethyl ammonium (PDDA) by electrostatic self-assembly to make the surface positively charged. Covalent bond modification refers to covalently linking some groups on the surface of 2D nanofluidics, thereby regulating the electronic structure and surface electrical properties of the nanofluidics. Ji *et al.*[50] grafted 1-aminopropyl-3-methylimidazolium bromide (APMIB) onto GO via carbodiimide, which also makes the surface positively charged. Fiber intercalation refers to the insertion of charged fibers between the layers of 2D nanofluidic membranes to increase the interlayer spacing and surface charge density, which is beneficial for improving the ion

selectivity and ion flux of nanochannels. For example, Chen *et al.*[51] obtained GO/aramid nanofibers (ANF) membranes with high surface charge density by compounding GO and ANF. Therefore, 2D nanofluidics can be endowed with excellent properties by the proper modification [Table 1].

Excellent ion regulation

The layered structure of 2D nanofluidic membranes can greatly reduce fluid flow resistance and maintain the characteristics of surface charge-regulated ion transport. The surface charge that controls ion transport. The ionic adjustment ability of 2D nanofluidic channels is affected by the distance between the layers because it determines the size and charge selectivity of the membranes. The force between the 2D nanosheets can ensure the formation of extremely small and uniform nanochannels (usually less than 5 nm). Compared with 1D nanochannels (usually greater than 10 nm), 2D nanochannels greatly reduce the channel size, which is conducive to the full coverage of the electric double layer (EDL) and improves the ability of ion transport regulation. In addition, ions and molecules with different sizes and charges can be separated for other applications by controlling the interlayer spacing[55]. For example, expanding the layer spacing to several nanometers can promote ultrafast water treatment, while reducing it to sub-nanometers can realize seawater desalination[56,57].

High flux

Ion flux is a key factor in determining the performance of 2D nanofluidic membranes. A higher ion flux promotes more ions to pass through in a certain period of time and produce a higher ion current[58]. 2D nanofluidic membranes contain many nanoscale or sub-nanoscale nanochannels, which contribute to the high ion flux. For example, GO membranes prepared by depositing GO nanosheets on polysulfone substrates coated with polydopamine have a membrane flux of 80-276 LMH/MPa, which is ~4-10 times higher than that of most commercial nanofiltration membranes[59]. The 5 μm thickness of the GO membrane prepared by Joshi *et al.*[60] also has a quite high membrane flux and almost perfect selectivity for molecules of a specific size. In addition, the membrane flux can be improved by increasing the porosity or reducing the thickness of the membranes, although the ion selectivity will inevitably be weakened. Therefore, it is necessary to achieve high ion flux while maintaining the surface charge-governed ion transport.

Ion transport properties of 2D nanofluidics

Ion selective transport

The pore diameter of 2D nanofluidic channels is generally below 3 nm, and they have structure and performance similar to or better than those of biological nanochannels, such as ion selective transport. The ion selective transport of nanofluidic channels means that channels only allow ions with opposite charges to the inner surface (counter ions) to pass through, while ions carrying the same charges to the inner surface (common ions) are repelled[61].

Ion transport regulation behavior is mainly caused by the nanoscale pore size and excessive charges on the inner surface of the nanochannels[62]. The internal surface charges adsorb counter ions to form an EDL to maintain the charge balance when the 2D nanofluidic membrane is immersed in an electrolyte solution. When the radius of the nanochannels is less than or equal to the thickness of the EDL, the EDL area will overlap with the entire channels [Figure 3A]. At this time, the ion transport behavior in the nanochannels is completely controlled by the surface charges due to the strong electrostatic interaction. The common ions are completely discharged from the nanochannels, and the counter ions become the only carriers, resulting in ion selective transport. When the radius of the charged nanochannels is larger than the thickness of the EDL, the control effect of surface charge on ion transport is weakened, and the ion selectivity of the

Table 1. Summary of surface functionalization methods of 2D nanofluidics

Surface functionalization methods	2D nanofluidics	Functional materials	Properties after functionalization	Ref.
Electrostatic self-assembly	MXene	PDDA	Surface positive electrification	[49]
Electrostatic self-assembly	MMT	Dioctadecyl dimethyl ammonium bromide	Temperature gating	[52]
Covalent bond modification	GO	APMIB	Surface positive electrification	[50]
Covalent bond modification	GO	Poly(N-iso-propylacrylamide)	Temperature gating	[53]
Fiber intercalation	GO	Silk nanofiber	Negative charge density enhancement	[48]
Fiber intercalation	GO	ANF	Negative charge density enhancement	[51]
Fiber intercalation	COF	ANF	Negative charge density enhancement	[54]

PDDA: Polydiallyl dimethyl ammonium; APMIB: 1-aminopropyl-3-methylimidazolium bromide; GO: graphene oxide; MMT: montmorillonite; ANF: aramid nanofibers.

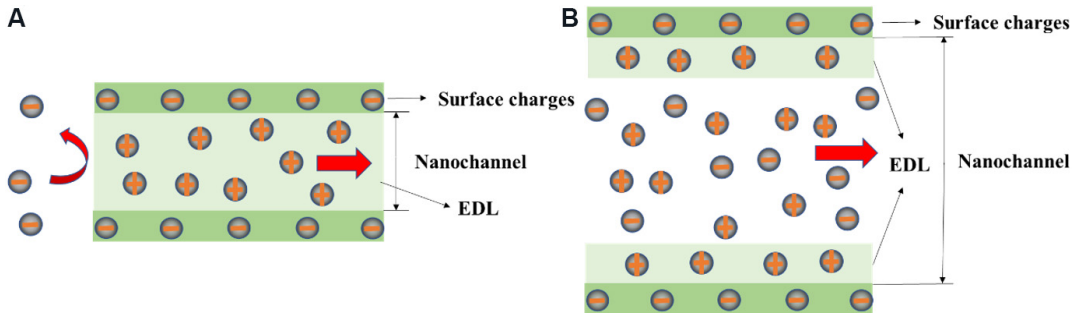

Figure 3. Effect of nanochannel radius on ion selective transport. (A) Schematic illustration of a nanochannel with a radius smaller (A) and larger (B) than the thickness of the EDL. EDL: Electric double layer.

nanochannels is reduced accordingly [Figure 3B]. Equation (1) gives the effective thickness ($d_{1/2}$) of an EDL[63]:

$$d_{1/2} \frac{1}{\sqrt{\frac{2n_d e^2}{\varepsilon\varepsilon_0 kT}}} \quad (1)$$

where n_d is the concentration of counter ions, e is the electronic charge, k is the Boltzmann constant, T is the temperature, ε is the dielectric constant of the solution and ε_0 is the influence constant. It can be concluded from Equation (1) that the effective thickness of the EDL increases with the decreasing concentration of counter ions [Figure 4A]. Therefore, the EDL area can cover the entire nanochannels to improve ion selectivity and promote ion transport at low concentrations. Therefore, it is easier for the EDL to completely cover the nanochannels at low concentrations and the ion selectivity of the nanochannels can be further improved.

Ultrafast ion transport

2D nanofluidics can also provide routes for ultrafast ion transport. Generally, the inner surface charges become dominant when the ratio of the inner surface area to the volume of the nanochannels increases, because a large part of the total charges are distributed on the inner surface of the nanochannels. On this

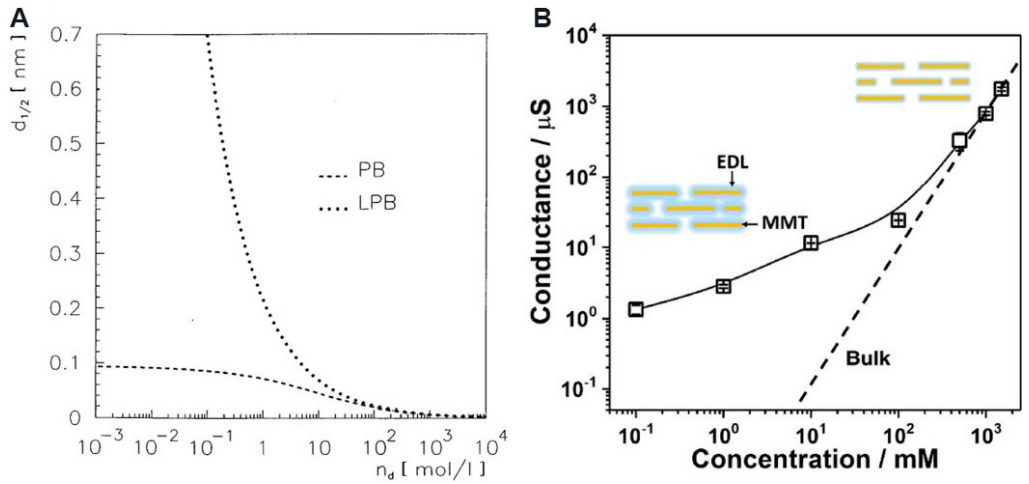

Figure 4. Relationship between thickness of EDL and ion concentration and the relationship between conductance and ion concentration. (A) Relationship between thickness of EDL and the counterion density. PB is the result of the nonlinear Poisson-Boltzmann theory and LPB is the result of the linearized Poisson-Boltzmann theory. Figure reproduced with permission from Schoch and Renaud[63] (Copyright © 2001 Elsevier). (B) Scatter line showing the change of the conductance of the nanochannels in different concentrations of KCl solution and straight line showing the conductance change of the bulk solution. Figure reproduced with permission from Wu *et al.*[52] (Copyright © 2020 Elsevier). EDL: Electric double layer.

basis, the inner surface charges of the nanochannels can strongly control the transport of ions at low concentrations[64]. This control is principally realized by the substantial surface charge increasing the ionic conductance in the nanochannels. Schoch *et al.*[36] simulated and measured the transport of ions in nanochannels filled with an electrolyte, as shown in Equations (2) and (3):

$$\gamma_{bulk} = 10^3(\mu_k^+ + \mu_{Cl}^-)cN_Ae \qquad (2)$$

$$G = 10^3(\mu_k^+ + \mu_{Cl}^-)cN_Ae(wh/d) + 2\mu_k^+\sigma_s^*(w/d) \qquad (3)$$

where γ_{bulk} is the electrical conductivity of the KCl bulk solution at 20 °C, μ_k^+ and μ_{Cl}^- are the mobility of K^+ and Cl^-, respectively, c is the electrolyte concentration, N_A is the Avogadro constant, G is the conductance in the nanochannels for all KCl concentrations, w is the width of the nanochannels, d is the length of the nanochannels, h is the height of the nanochannels and σ_s^* is the effective surface charge density. The conductance in the nanochannels is determined by the first term in Equation (3) when the solution concentration is high; otherwise, it is determined by the second term in Equation (3). Therefore, the conductance in the nanochannels is several orders of magnitude higher than that of the bulk solution at low concentration, which is conducive to promoting ion transport and generating ion current [Figure 4B][52]. The insets of Figure 4B depict the distribution of the EDL in MMT nanochannels at high and low concentrations. It can be seen that the nanochannels are completely covered by the EDL at low concentrations, indicating that the nanochannels can simultaneously achieve ion conductance-influenced ultrafast ion transport and EDL-influenced ion selective transport.

CONSTRUCTION OF 2D NANOFLUIDICS

In order to use 2D nanofluidics for blue energy harvesting, 2D materials need to be prepared as ISMs with excellent ion selectivity and high ion flux, exploiting the nanoscale pores and inner surface charges of nanochannels between 2D nanosheet layers to control ion-directed transport. Therefore, the construction of 2D nanofluidics is necessary to achieve efficient blue energy harvesting.

Common construction methods for 2D nanofluidic membranes include vacuum filtration, interfacial polymerization, *in situ* growth, chemical vapor deposition and so on[65-68]. Vacuum filtration refers to the injection of a certain concentration of 2D nanosheet dispersion into a filtration device and filtering under negative pressure to obtain membranes with a layered structure [Figure 5A]. The structure of the membranes obtained by the vacuum filtration method is compact and uniform, and the thickness can be adjusted according to the concentration or volume of the dispersion. Interfacial polymerization utilizes two highly reactive monomers to polymerize at the interface of two immiscible solvents, resulting in 2D membranes on porous substrates [Figure 5B]. *In situ* growth refers to directly putting the substrate into the precursor of the membrane to make the 2D material grow on the surface of the substrate. Although the in-situ growth method generally has a long reaction period, the structure of the prepared membrane is dense and uniform [Figure 5C]. Chemical vapor deposition mainly utilizes one or several vapor phase compounds or elements to perform chemical reactions on the substrate surface to form membranes. Large-scale membranes with excellent properties can be obtained by this method [Figure 5D].

At present, some typical materials, such as carbon materials, clay materials, MXenes and so on, have been widely used to construct 2D nanofluidic membranes due to their charged surfaces, easy exfoliation and well-structured nanochannels of the constructed membranes. In addition, emerging 2D materials, such as COFs, are also utilized to construct 2D nanofluidic membranes due to their high porosity, excellent pore structure and uniform and tunable pore size. The preparation methods of 2D nanofluidic membranes based on different materials are discussed in the following sections.

Carbon-based 2D nanofluidics

Carbon-based 2D nanofluidic materials mainly include graphene and GO. There are two main strategies for the production of graphene[70]. The first one is a bottom-up method, such as chemical vapor deposition, which is mainly realized by the chemical decomposition of carbon sources (such as methane, ethanol and so on) at a certain temperature or external field and deposition on the substrate surface. The reaction substrates are generally metal (Cu, Ni and so on) and non-metallic (SiO_2, Si_3N_4 and so on). The external conditions that need to be controlled include temperature, pressure, gas flow rate and so on. For example, Li *et al.*[71] prepared large-area graphene membranes on Cu substrates by chemical vapor deposition using methane as a carbon source. Kim *et al.*[69] synthesized graphene membranes on nickel substrates by chemical vapor deposition.

The second strategy is a top-down method, in which single-layer graphene is exfoliated from the bulk graphite by mechanical exfoliation[72]. Since no chemical reaction is involved, the surface of the single-layer graphene obtained by this method is clean. However, the amount of single-layer graphene prepared by this method is limited and the preparation process is tedious, so it cannot be used for large-scale production[73]. For this reason, Jayasena and Subbiah[74] reported another method of mechanical exfoliation, in which a diamond wedge was used to scrape graphene from the highly ordered pyrolytic graphite, with ultrasonic oscillation used as an assistant to peel off. By controlling the frequency of ultrasonic oscillation, the properties of the prepared single-layer graphene tend to be consistent.

GO is the oxidized form of graphene and is usually synthesized by chemical exfoliation, where graphite is oxidized by strong oxidants to form hydrophilic groups at the graphite lamellar and edge. The oxidized graphite is then peeled off under the action of ultrasonic treatment or pyrolysis expansion and dispersed in the solvent to form a single- or multi-layer GO dispersion liquid. Hummers and Richard[75] used strong oxidants, such as potassium permanganate and sodium nitrite, to chemically peel graphite into GO. The GO obtained by this method has a high degree of oxidation and takes a short time. However, there are many

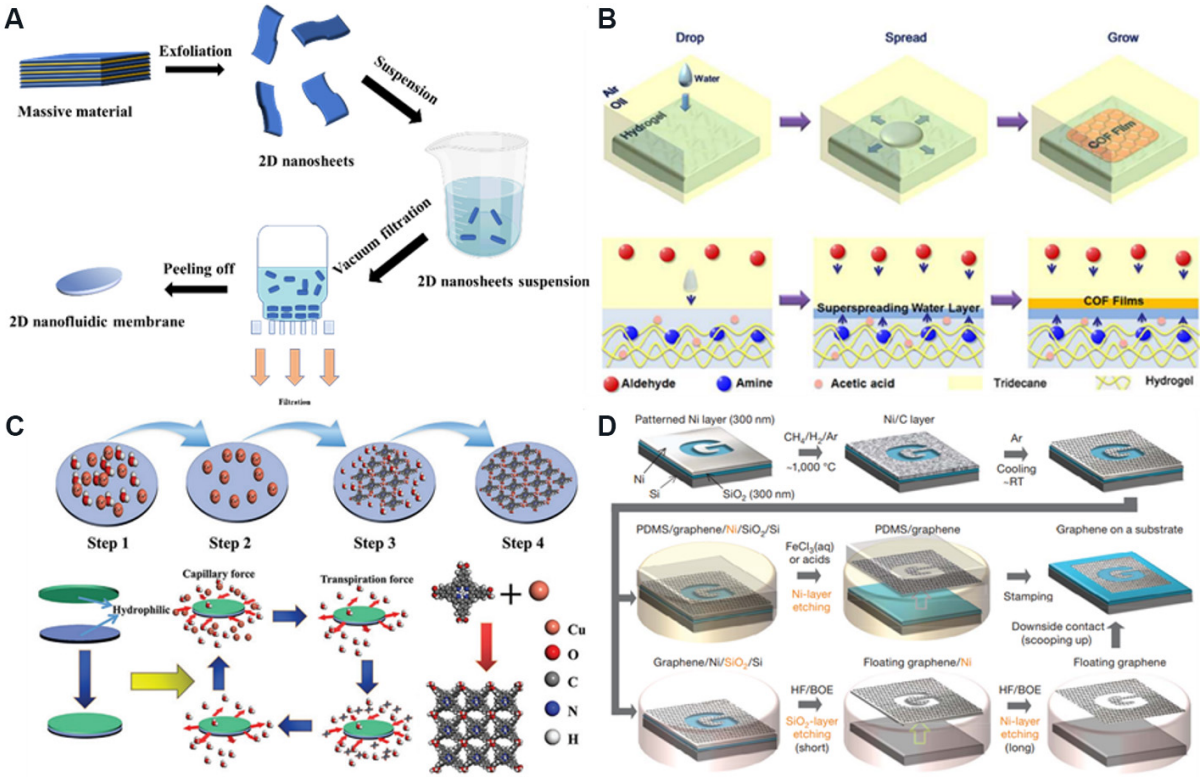

Figure 5. Preparation methods of 2D nanofluidic membranes. (A) Vacuum filtration. (B) Interfacial polymerization. Figure reproduced with permission from Hao *et al.*[65] (Copyright © 2018 American Chemical Society). (C) *In situ* growth. Figure reproduced with permission from Liu *et al.*[66] (Copyright © 2021 Wiley). (D) Chemical vapor deposition. Figure reproduced with permission from Kim *et al.*[69] (Copyright © 2009 Nature).

factors that need to be controlled in this method, and toxic gases are produced in the preparation process. Marcano *et al.*[76] improved the above method. They used potassium permanganate as the oxidant to exfoliate bulk graphite in a 9:1 mixture of H_2SO_4/H_3PO_4, which improved the oxidation efficiency, and there was no toxic gas in the preparation process and the regularity of GO was higher.

Clay-based 2D nanofluidics

Clay-based 2D nanofluidic materials mainly include zeolites, vermiculite, hydrotalcite, MMT and so on. Zeolites are aluminosilicate minerals that contain alkali metals or alkaline earth metals and are widely used in the fields of catalysis, adsorption, separation and so on[77-80]. There are many methods for the preparation of 2D zeolite nanosheets, such as hydrothermal synthesis. Agrawal *et al.*[81] reported that zeolite nanosheets/polystyrene nanocomposites were synthesized by hydrothermal synthesis using molten polystyrene and zeolite precursors. They carried out ultrasonic treatment and centrifugation in organic solvents, such as toluene, to remove polymers and large particles to form monolayer zeolite nanosheets. The monolayer zeolite nanosheets are then filtered in a vacuum to form a membrane. However, there is reversibility in hydrothermal synthesis, and some 2D zeolite membranes with special structures cannot be synthesized by hydrothermal synthesis. A novel zeolite synthesis route known as the assembly-disassembly-organization-reassembly (ADOR) method can avoid the disadvantages of hydrothermal synthesis[82]. Firstly, the initial block 3D zeolite is prepared (assembly), then the bulk zeolite is exfoliated into 2D separation layers (disassembly), and then these layers are organized in a suitable way (organization). Finally, a novel 3D zeolite with new topological structures is obtained by calcination (reassembly). Mazur *et al.*[83] prepared two different types of 2D zeolites by the ADOR method, which makes it possible to prepare materials with the

same layer topology but different layer connectivity.

Layered bimetallic hydroxide (LDH) is a general term for hydrotalcite and hydrotalcite-like compounds. Its chemical composition can be expressed as $[M_{1-x}^{2+}M_x^{3+}(OH)_2]^{x+}\cdot[A_{n-x/n}]\cdot mH_2O$, where M represents metal cations and A represents anions[84]. Traditional LDH membranes can be prepared by the exfoliation-reconstruction method. Firstly, the bulk LDH is exfoliated into single-layer nanosheets [Figure 6A], and then the LDH nanosheets with a uniform thickness are filtered to form a membrane. For example, Konch *et al.*[85] obtained 2D LDH nanosheets by exfoliating a CoAl LDH and then prepared the LDH membrane by vacuum filtration, which can be used for osmotic energy conversion. LDH nanofiltration and ultrafiltration membranes for seawater desalination can be prepared by phase conversion[86].

Vermiculite is a layered silicate clay mineral. 2D vermiculite membranes can also be prepared by the exfoliation-reconstruction method. Shao *et al.*[87] exfoliated vermiculite into several layers of vermiculite nanosheets through ion exchange in water and then reconstructed them into 2D layered membranes through vacuum filtration [Figure 6B]. The resulting membrane has high proton conductivity and extraordinary thermal stability. Gogoi and Raidongia[88] prepared a vermiculite membrane with independent repair ability through the exfoliation-reconstruction method, which has broad application prospects in water desalination, energy storage and so on.

MMT is another commonly used clay mineral composed of negatively charged silicate layers with nanometer thickness depending on the electrostatic interaction between layers. The preparation of 2D MMT membranes is mainly achieved by the exfoliation-reconstruction method. MMT membranes can be chemically modified to obtain desirable characteristics. Huang *et al.*[89] prepared MMT membranes with high water permeability and acid-base stability, and these were widely used in nanofiltration. Using the natural cation exchange between dioctadecyl dimethyl ammonium and MMT, our group successfully prepared a temperature- and voltage-responsive layered membrane with 2D nanofluidic channels by vacuum filtration [Figure 6C], which provides a novel strategy for the synthesis of intelligent response 2D membranes[90].

MXene-based 2D nanofluidics

As novel 2D materials, MXenes are usually expressed as $M_{n+1}X_nT_x$ (n = 1-3), where M is a transition metal (e.g., titanium, vanadium, chromium, niobium and so on) and X refers to C or N, and T_x can be functional groups, such as carboxyl or carbonyl groups. MXenes can be obtained by etching the A layer of MAXs, such as Ti_2AlC, where A refers to a group of elements (such as aluminum, silicon and so on)[91].

Etching MAX phases with hydrofluoric acid (HF) is the most commonly used method to prepare MXenes. Naguib *et al.*[92] use an HF aqueous solution to peel off the MAX powder and produce MXene nanosheets by ultrasonic treatment. However, the yield of single-layer MXene nanosheets prepared by this method is low. For this reason, HF etching combined with ion or organic molecular intercalations can be used to insert ions or organic molecules into the interlayers of MXenes etched by HF to increase the interlayer spacing and improve the exfoliation efficiency. Lipatov *et al.*[93] reported a method of Li^+ insertion for assisted exfoliation. Firstly, the bulk MAX was etched with a mixture of HCl and LiF, and then the pH value was adjusted to ~6. Monolayer or multilayer $Ti_3C_2T_x$ nanosheets can be prepared in high yields, as shown in Figure 7. In addition, since the insertion of Li^+ increases the interlayer spacing, ultrasonic treatment is not required.

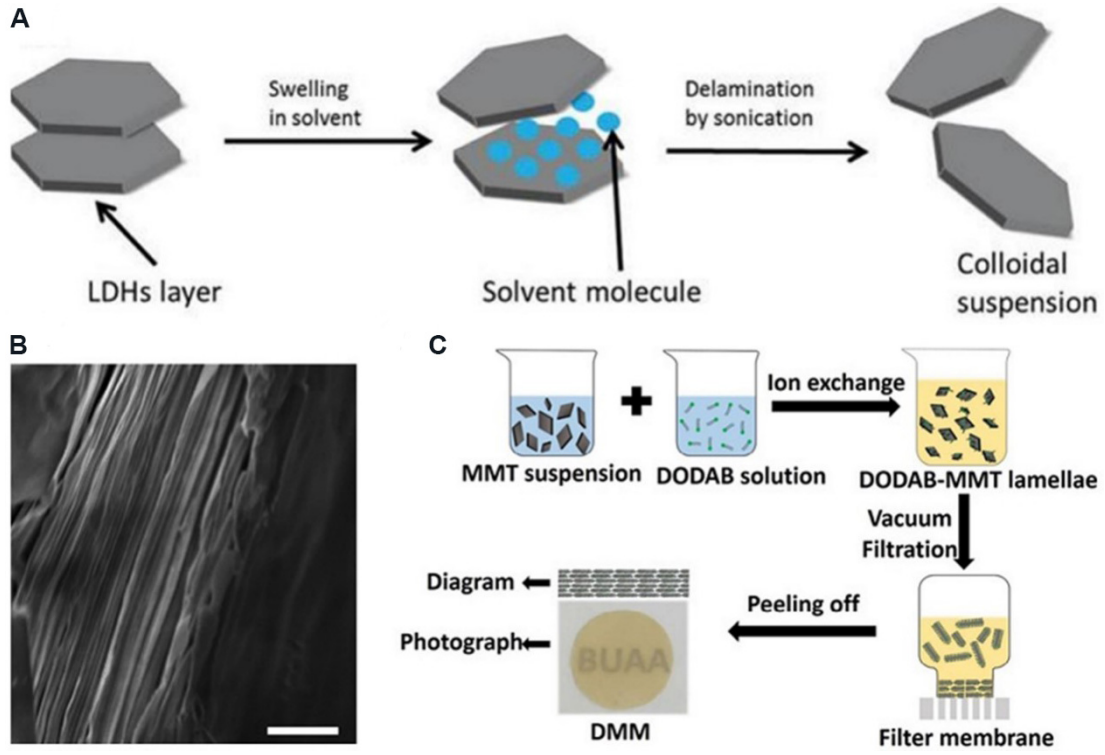

Figure 6. Preparation of clay-based 2D nanofluidic membranes. (A) Exfoliation process of bulk LDH. Figure reproduced with permission from Lu *et al.*[84] (Copyright © 2018 Elsevier). (B) Cross-section scanning electron microscopy image (scale bar: 1 μm) showing a layered microstructure. Figure reproduced with permission from Shao *et al.*[87] (Copyright © 2015 Nature). (C) Schematic of double-layer intercalated MMT membrane preparation process. Figure reproduced with permission from Xiao *et al.*[90] (Copyright © 2017 American Chemical Society). LDH: Layered bimetallic hydroxide; MMT: montmorillonite; DODAB: dioctadecyl dimethyl ammonium bromide.

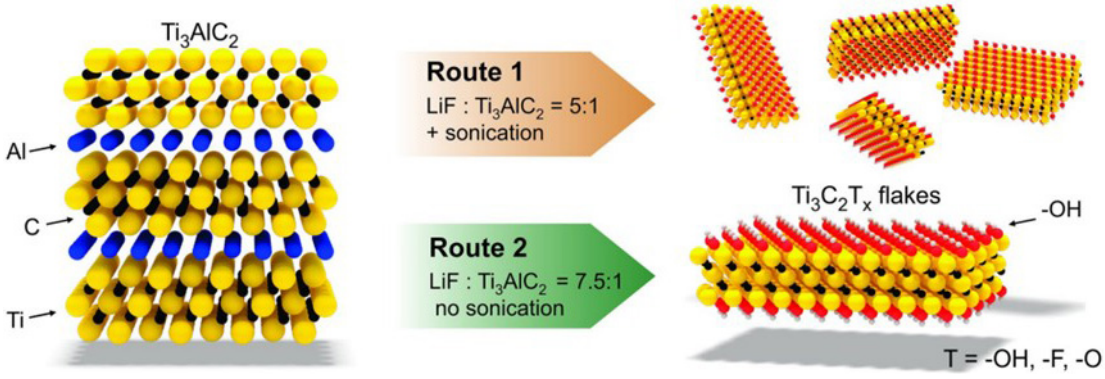

Figure 7. MXenes prepared by exfoliating Ti_3AlC_2 in a mixture of HCl and LiF without ultrasonic treatment. Figure reproduced with permission from Lipatov *et al.*[93] (Copyright © 2016 Wiley).

COFs and metal-organic frameworks

COFs refer to porous crystalline materials formed by symmetrically connecting organic junctions with light atoms (hydrogen, boron, carbon and so on) through covalent bonds. Considering their large specific surface area, low density, superior thermal stability and controllable microporous structure, COFs have shown promising applications in gas adsorption, heterogeneous catalysis, energy storage and so on[94]. The structure of a COF can be designed according to topology and channels with different shapes and sizes can

be obtained by using monomer units with different shapes, sizes and connecting groups[95]. According to the shape, channels can be divided into hexagonal, diamond and triangular channels [Figure 8A-I].

Mechanical exfoliation is frequently used to prepare COF nanosheets. For example, Chandra *et al.*[105] synthesized eight different COF powders by a solvothermal aldehyde-amine Schiff base condensation reaction. After mechanically grinding these COF powders in methanol for 30 min, 2D COF nanosheets with a thickness of several nanometers were obtained. Berlanga *et al.*[106] carried out an ultrasonic treatment of layered crystals of COF-8 in dichloromethane and 2D COF nanosheets with a thickness of 4 nm were obtained by centrifuging the resulting suspension [Figure 8J]. COF-based 2D nanofluidic membranes can be produced by the vacuum filtration of COF nanosheets. In addition, interfacial polymerization is also a common method to synthesize COF membranes. Dey *et al.*[107] used trialdehyde-based phloroglucinol as the organic phase monomer and four amines, including 4,4'-azodiphenylamine, as the aqueous monomer and reacted at the oil-water interface for 72 h to obtain defect-free self-supported COF membranes. Wang *et al.*[108] used 1,3,5-triformylphloroglucinol as the organic phase monomer and benzidine as the aqueous phase monomer to fabricate substrate-supported COF membranes by in-situ interfacial polymerization on a porous polymer substrate.

In addition, there are 2D nanofluidic materials [i.e., metal-organic frameworks (MOFs)] similar in structure to COFs. MOFs are crystalline porous materials with periodic network structures formed by inorganic metal centers (metal ions or clusters) and bridged organic ligands through self-assembly. MOFs have been used in the fields of catalysis and energy storage because of their large surface area and high porosity[109,110].

There are two main strategies for preparing 2D MOF nanosheets: the top-down method and the bottom-up method. The top-down method involves destroying the interlayer interaction of the bulk MOF, such as weak van der Waals forces, to obtain single- or several-layer 2D MOF nanosheets. Gallego *et al.*[111] reported the synthesis of 2D MOF nanosheets by solvent-assisted exfoliation. Wang *et al.*[112] reported that a layered MOF was peeled off by a freeze-thaw method in a suitable solvent [Figure 9] and large and defect-free MOF nanosheets were obtained. In addition, the exfoliation process can be facilitated by grinding and ultrasonic treatment[113]. The bottom-up method refers to the direct formation of 2D MOF nanosheets using metal ions and organic ligands. For example, Makiura *et al.*[114] reported that MOF nanosheets could be synthesized by surface-restricted growth. A mixture of CoTCPP and pyridine was dispersed in a $CuCl_2 \cdot 2H_2O$ aqueous solution. By controlling the deposition process of the mixture on the substrate, MOF nanosheets with different thicknesses were produced.

Transition metal sulfides

Due to its unique layered structure (monolayer Mo atoms sandwiched between two layers of S atoms) and adjustable bandgap, MoS_2 is widely used in energy storage devices, such as supercapacitors and lithium batteries[115,116]. Furthermore, MoS_2 nanosheets can be used to prepare 2D nanofluidic membranes for osmotic energy conversion because of their surface electrification and ultrathin thickness.

MoS_2 2D nanofluidic membranes are prepared by the exfoliation-reconstruction method and other materials can be added to the preparation process for chemical modification or the preparation of composite membranes. For example, Zhu *et al.*[117] mixed a dispersion of chemically delaminated MoS_2 nanosheets with cellulose nanofiber (CNF) suspensions to prepare a MoS_2/CNF composite membrane by vacuum filtration. Cheng *et al.*[118] obtained MoS_2 nanosheets by peeling off bulk powders in a triethanolamine solution and then added MoS_2 nanosheets to a polyamide acid solution for thermal imidization to prepare a MoS_2/polyimide (PI) composite membrane [Figure 10].

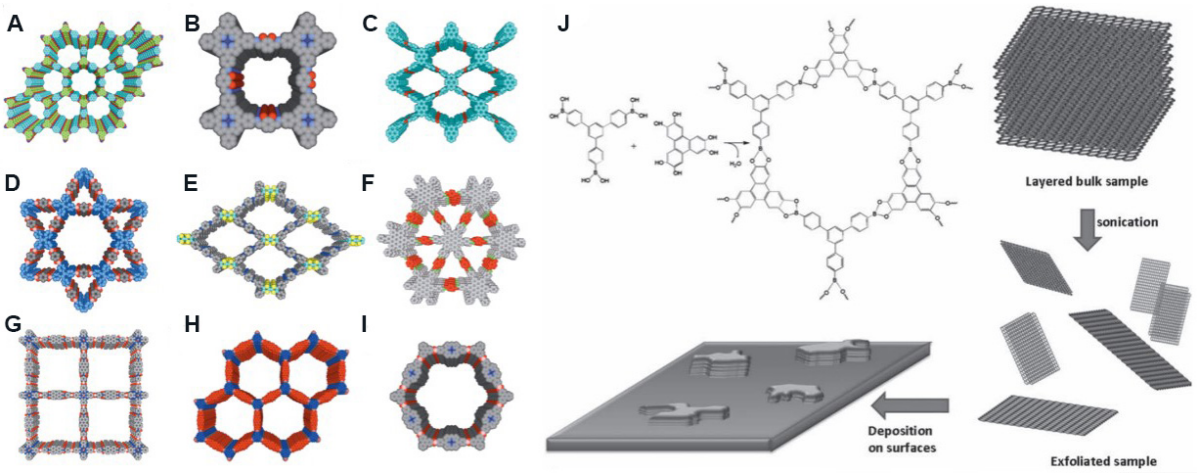

Figure 8. Different pore structures of COFs and the preparation process of COF nanosheets. (A) TP-COF. Figure reproduced with permission from Wan *et al.*[96] (Copyright © 2008 Wiley). (B) 2,3 DhaTph-COF. Figure reproduced with permission from Shinde *et al.*[97] (Copyright © 2014 Royal Society of Chemistry). (C) Py azine-COF. Figure reproduced with permission from Dalapati *et al.*[98] (Copyright © 2013 American Chemical Society). (D) TPE Ph-COF. Figure reproduced with permission from Dalapati *et al.*[99] (Copyright © 2016 American Chemical Society). (E) TTF Ph-COF. Figure reproduced with permission from Jin *et al.*[100] (Copyright © 2014 Wiley). (F) HBC-COF. Figure reproduced with permission from Dalapati *et al.*[101] (Copyright © 2015 Nature). (G) D_{CuPc}-A_{DI}-COF. Figure reproduced with permission from Jin *et al.*[102] (Copyright © 2013 Wiley). (H) D_{TP}-A_{NDI}-COF. Figure reproduced with permission from Jin *et al.*[103] (Copyright © 2013 Royal Society of Chemistry). (I) TP-Por-COF. Figure reproduced with permission from Calik *et al.*[104] (Copyright © 2014 American Chemical Society). (J) Preparation of COF nanosheets by mechanical exfoliation. Figure reproduced with permission from Berlanga *et al.*[106] (Copyright © 2019 Wiley). COFs: Covalent organic frameworks.

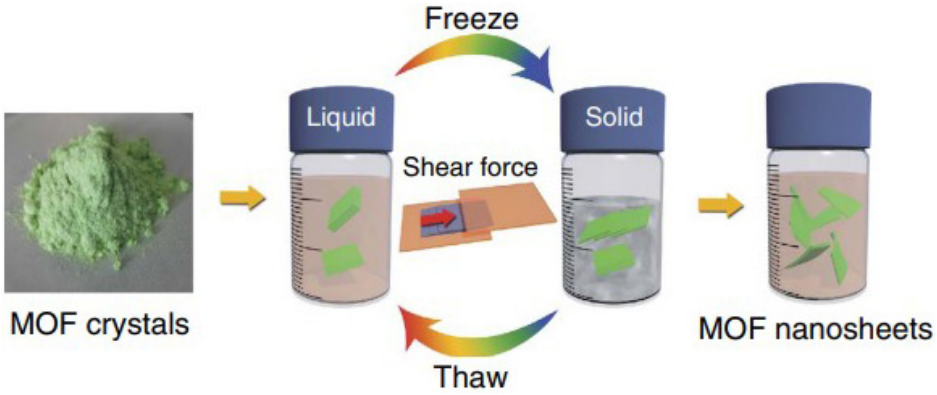

Figure 9. Freeze-thaw exfoliation of MOF crystals to form dispersed nanosheets. Figure reproduced with permission from Wang *et al.*[112] (Copyright © 2017 Nature).

2D NANOFLUIDICS FOR BLUE ENERGY HARVESTING

In recent years, 2D nanofluidics have been widely applied to blue energy harvesting, primarily based on salinity gradient- and pressure-driven systems.

Salinity gradient-driven 2D nanofluidic generators

Working principle

Salinity gradient-driven 2D nanofluidic generators refer to energy harvesting from the ion concentration diffusion, with these devices therefore also known as concentration cells. The configuration of a concentration cell is based on two solutions with different salinities separated by an ion-selective 2D nanofluidic membrane [Figure 11][119]. Under the salinity gradient, the ions transport through the

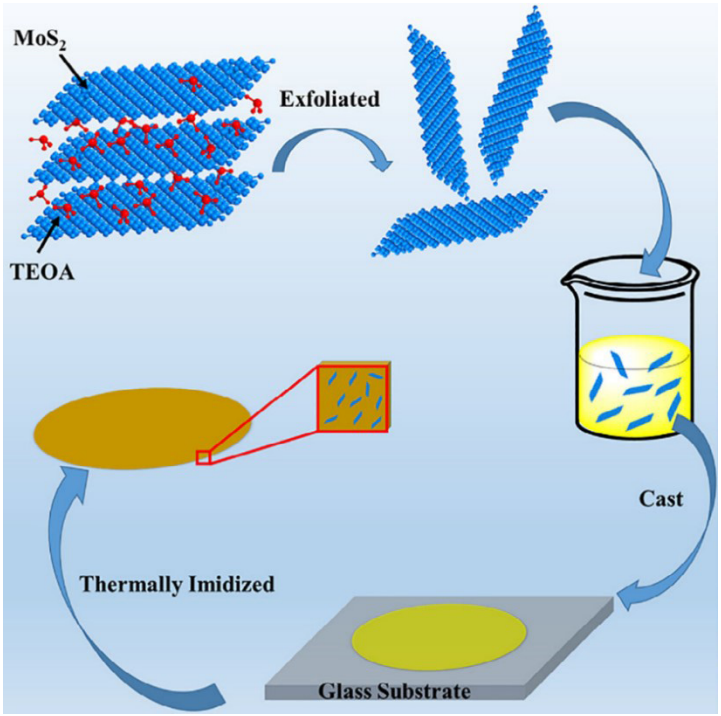

Figure 10. Preparation of MoS_2/PI composite membrane. Figure reproduced with permission from Cheng *et al.*[118] (Copyright © 2019 Wiley).

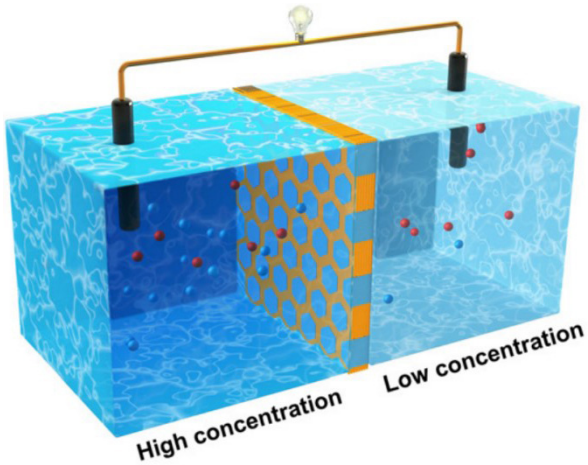

Figure 11. Schematic diagram of power generation principle of concentration cell based on 2D nanofluidic membranes. Figure reproduced with permission from Hou *et al.*[119] (Copyright © 2021 Wiley).

membrane from the high concentration side to the low concentration one, which creates a transmembrane electric potential difference. To maintain the electrical neutrality of the two solutions, electrochemical redox reactions take place on the electrode surface. Electrons transfer from the anode to the cathode through an external circuit to form an electric current, generating electric energy and supplying power to the load. This process is also known as reverse electrodialysis (RED). The electrodes used in concentration cells are usually a pair of Ag/AgCl electrodes.

Assuming that the concentration of the solution on both sides of the ion exchange membrane is c_H (high concentration) and c_L (low concentration), respectively, the composition of the concentration cell is shown in Equation (4):

$$Ag \mid AgCl(s) \mid NaCl(c_H) \parallel NaCl(c_L) \mid AgCl(s) \mid Ag \quad (4)$$

The electrode reactions of the positive and negative electrodes are shown in Equations (5) and (6):

$$(-)\ Ag + Cl^-(c_H) - e^- \rightarrow AgCl \quad (5)$$

$$(+)\ AgCl + e^- \rightarrow Ag + Cl^-(c_L) \quad (6)$$

The total electrode reaction is shown in Equation (7):

$$Cl^-(c_H) \rightarrow Cl^-(c_L) \quad (7)$$

Therefore, the electrode reaction of the concentration cell is the transformation of Cl^- from high to low concentration. The electrode reaction can take place as long as the concentration difference between the two sides of the ion exchange membrane is maintained.

The currently studied power output of the osmotic energy conversion process is usually limited due to the lack of high-performance ISMs. Therefore, the key to the rational and efficient utilization of osmotic energy is the introduction of ISMs. 2D nanofluidic membranes with controllable ion transport behavior and high ion flux can achieve high-performance RED, and the performance of the membranes can be improved by various methods of preparation and optimization to promote the efficient utilization of renewable osmotic energy[120].

Application examples

Graphene and its derivatives are vital materials for the preparation of ISMs for concentration cells due to their rich surface charge, extremely thin layer thickness and excellent ion selectivity. Sun *et al.*[121] utilized GO-based 2D nanofluidic membranes for osmotic power generation, explained the mechanism of transmembrane potential generation and measured the generated voltage in a self-made device to evaluate the energy conversion characteristics [Figure 12A]. They observed significant differences in voltages produced by different types of metal ions [Figure 12B] and stated that larger differences in mobility between cations and anions might produce greater voltages.

Clay-based 2D nanofluidic membranes have been widely studied because of their low cost and simple fabrication. Cheng *et al.*[122] chemically modified pre-exfoliated kaolinite with bis-(γ-triethoxysilylpropyl)-tetrasulfide (Si-69) and then obtained a reconstituted kaolinite membrane (RKM) by vacuum filtration. RKM has obvious surface charge-controlled ion transport behavior and near-perfect cation selectivity. In different concentrations of KCl solutions, the current-voltage response of a 25 μm-thick RKM is linear [Figure 12C]. In addition, an increase in salinity gradient and pH can promote the generation of net diffusion current [Figure 12D]. Under neutral conditions (pH 6) and a 100 times concentration difference, the output power density of the concentration cell based on the RKM reached 0.18 W/m^2.

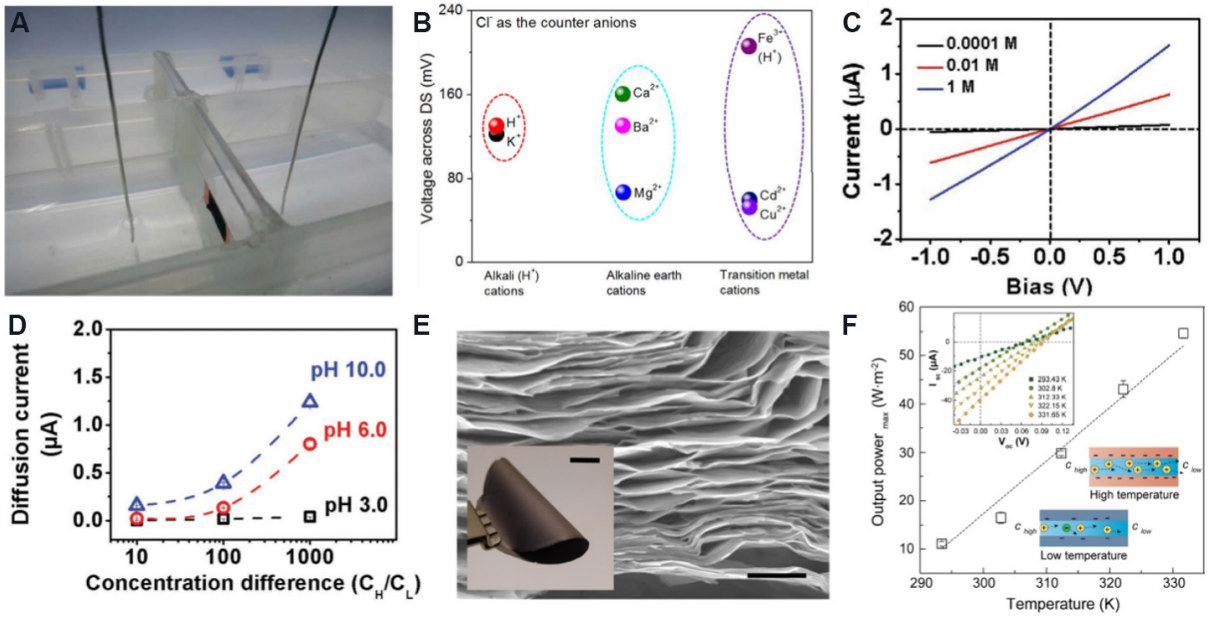

Figure 12. Different types of 2D nanofluidic membranes for osmotic power generation. (A) Voltage measurement installation. (B) Magnitude of voltage produced by different cations. Figures reproduced with permission from Sun *et al.*[121] (Copyright © 2019 Nature). (C) I-V response at different KCl concentrations. (D) Variation of diffusion current with concentration gradient and pH. Figures reproduced with permission from Cheng *et al.*[122] (Copyright © 2017 Wiley). (E) Cross-sectional SEM image of layered $Ti_3C_2T_x$ membrane (scale: 1 μm). Inset shows $Ti_3C_2T_x$ membrane with a thickness of 3 μm, illustrating the excellent flexibility of the membrane (scale: 10 mm). (F) Maximum output power density at different temperatures. Inset shows I-V characteristic curve at different temperatures. Figures reproduced with permission from Hong *et al.*[123] (Copyright © 2019 American Chemical Society).

As a new type of 2D nanofluidic membrane, MXene-based membranes have also been widely studied in concentration cells. Hong *et al.*[123] etched a MAX (Ti_3AlC_2) with a mixture of LiF and HCl to obtain MXene nanosheets and then prepared an MXene layered membrane by vacuum filtration. Figure 12E shows a cross-sectional SEM image of the lamellar membrane and its clear layered structure. At a 1000 times salinity gradient, the output power density of the MXene membrane is as high as 21 W/m² and the energy conversion efficiency is 40.6%. In addition, this group also explored the effect of heat treatment on the output power density. It was found that the output power density increases with increasing temperature in the temperature range of 294-341 K, and the output power density of 54 W/m² is obtained at 331 K [Figure 12F]. This is the result of the increase in the local concentration and mobility of cations on the charged surface, with the membrane still maintaining stable chemical and mechanical properties after the increase in temperature.

The narrow space of the nanochannels formed by simply stacking the nanosheets leads to a slow ion transport rate and power density. For this reason, the performance of membranes can be improved by preparing composite membranes. Wu *et al.*[124] prepared a GO/CNF composite membrane, which improved the ion transport capacity of 2D nanofluidic channels. CNFs have high-density functional groups and excellent mechanical properties. By compounding CNFs with GO nanosheets, the narrow channels can be enlarged and the energy barrier of ion transport reduced. Furthermore, negative charges are introduced between GO nanosheets to maintain high ion selectivity. Compared with a pure CNF or GO membrane, the output power density and current density of the GO/CNF composite membrane are increased, as shown in Figure 13A and B. By mixing artificial seawater (0.5 M NaCl) and river water (0.01 M NaCl), the maximum output power density of the membrane reached 4.19 W/m².

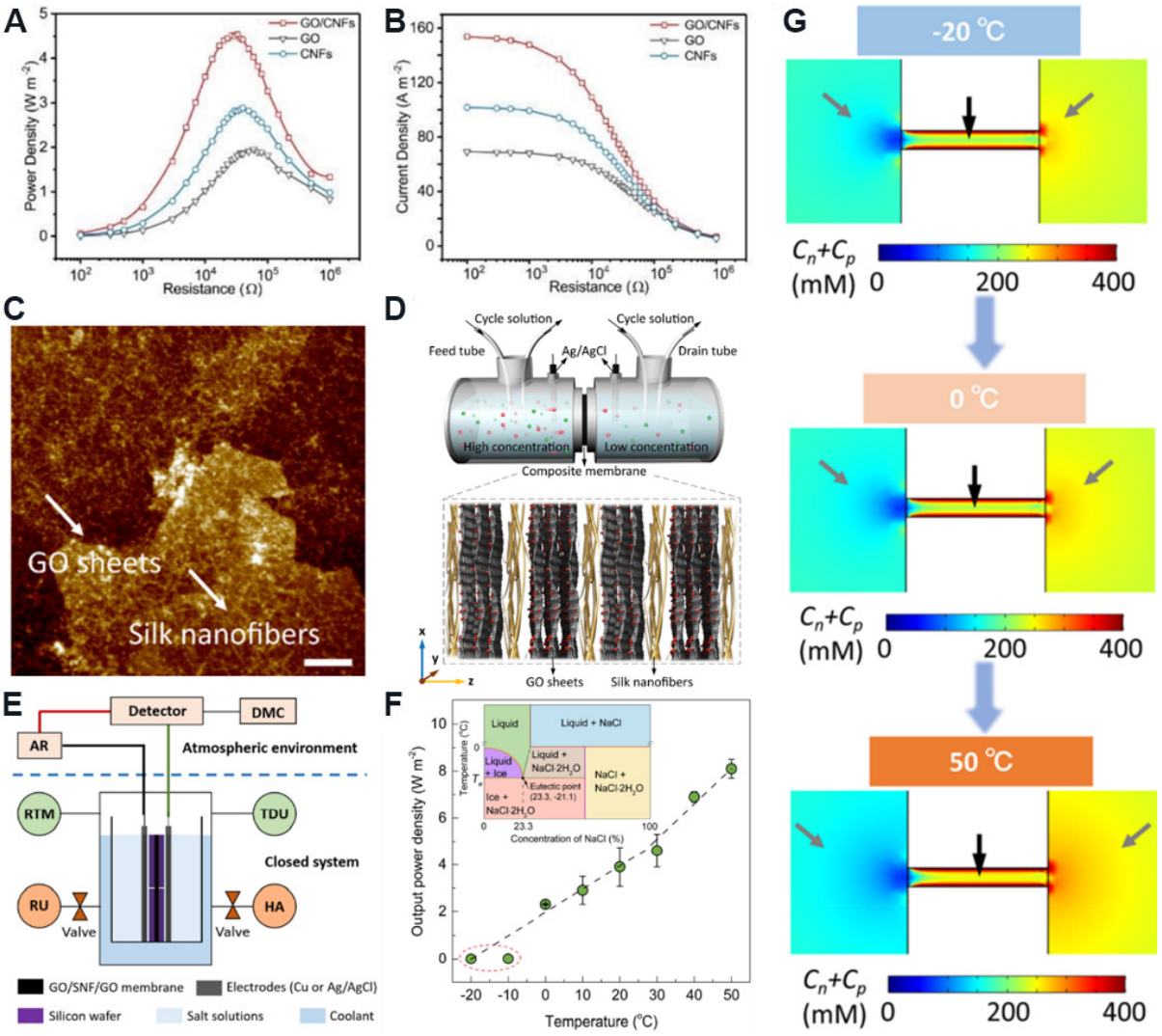

Figure 13. Performance and theoretical simulation diagram of concentration cell based on GO-based composite membranes. (A) Output power density and (B) output current density of GO/CNF composite membrane are higher than that of a pure CNF or GO membrane. Figures reproduced with permission from Wu *et al.*[124] (Copyright © 2018 Royal Society of Chemistry). (C) Structure of GO/SNF/GO composite membrane (scale: 500 nm). (D) Schematic diagram of GO/SNF/GO composite membrane and its concentration cell. (E) Heating device. (F) Variation of output power density with temperature. The inset shows the phase diagram for aqueous sodium chloride (NaCl-H_2O) at constant pressure. (G) Numerical simulation diagram of ion concentration distribution at different temperatures. Figures reproduced with permission from Xin *et al.*[48] (Copyright © 2020 American Chemical Society). GO: Graphene oxide; CNF: cellulose nanofiber.

Xin *et al.*[48] designed a sandwich-structured GO/SNF/GO composite membrane, in which the 1D SNFs can inhibit the free slip of GO [Figure 13C], so that the membrane maintains excellent mechanical properties and long-term stability. The two compartments of the concentration cell designed by the team are connected to the circulating solution [Figure 13D], which can maintain the concentration gradient by constantly replenishing and discharging the solution and achieve continuous power generation. The output power density of the concentration cell reaches 5.07 W/m^2 at a 50 times salinity gradient. In addition, the authors designed a heating device that can simulate a low-temperature environment to monitor the effect of different temperatures on the output power density [Figure 13E]. Figure 13F shows that the output power density increases with increasing temperature. This is caused by the increase of ion concentration in the nanochannel at high temperature, as confirmed by numerical simulations based on the Poisson and Nernst-

Planck equation, which depicts the ion concentration distribution at different temperatures [Figure 13G].

Recently, some additives have been introduced into 2D nanofluidics to improve their membrane mechanical strength and surface charge density. For instance, Zhang *et al.*[27] prepared an MXene/ANF composite membrane [Figure 14A] that exhibited outstanding cationic selectivity and osmotic energy conversion performance. Figure 14B depicts the power generation performance of the composite membrane with 11% ANF by weight in a concentration cell composed of artificial sea and river water. With increasing resistance, the current density on the external circuit decreases and the output power density is 3.7 W/m^2. In addition, the maximum power density of the MXene/ANF composite membrane in natural seawater (0.6 M NaCl) and river water (0.004 M NaCl) system can reach ~4.1 W/m^2.

Composite 2D nanofluidic membranes based on COFs have also been intensively studied for osmotic energy power generation. Man *et al.*[54] prepared a PyPa-SO_3H/SANF composite membrane using sulfonated 2D COF (PyPa-SO_3H) nanosheets and styrene sulfonic sodium-grafted aramid nanofibers (SANFs) to achieve high-performance osmotic energy conversion. The SEM image of the composite membrane [Figure 15A] shows that the membrane has an ultrathin thickness and layered structure. The X-ray diffraction pattern [Figure 15B] confirms that PyPa-SO_3H has high crystallinity, and the illustration shows the conformation of PyPa-SO_3H staggered stacking. The remarkable feature of COF membranes is that they have rich 1D nanofluidic channels in the direction perpendicular to the nanosheets and 2D nanofluidic channels in the direction parallel to the nanosheets. Therefore, compared with the complex ion transport across the membrane in traditional 2D nanofluidic membranes [Figure 15C], the 1D and 2D channels of the COF membrane make the ion transport distance shorter and the flux higher through the synergistic effect, as shown in Figure 15D and E. Furthermore, SANFs further improved the ion selectivity and mechanical strength of the membrane and enhanced the performance of the ion rectifier. When the PyPa-SO_3H/SANF composite membrane is applied to the concentration cell, the output power density of 9.6 W/m^2 can be obtained in the natural seawater/river water system [Figure 15F], which is much higher than the commercial standard (5 W/m^2).

In addition to using 2D nanofluidic membranes with a single charge to construct concentration cells, 2D nanofluidic membranes with opposite charges can be connected in series to construct concentration cells to generate efficient charge separation, a superimposed electrochemical potential difference and ion flux caused by bidirectional ion diffusion, thus providing a higher output power density. Ji *et al.*[50] coupled positively-charged APMIB to GO nanosheets by a carbodiimide-catalyzed coupling reaction and adjusted the surface charge polarity of 2D nanochannels from negative (-123 mC/m^2) to positive (+147 mC/m^2) to prepare graphene oxide membranes (GOMs) with opposite charge. A pair of GOMs with opposite charges were placed in a three-chamber electrochemical concentration cell filled with high- and low-concentration electrolyte solutions [Figure 16A]. By mixing artificial sea and river water, an output power density of 0.77 W/m^2 could be obtained. The concentration cell based on the oppositely charged GOMs in series could directly power low-power electronic devices, as shown in Figure 16B and C.

Ding *et al.*[49] modified MXene nanosheets with PDDA to prepare an MXene membrane with a positive charge on the surface and designed a concentration cell by arranging the positively charged MXene membrane and a negatively charged MXene membrane in series [Figure 16D]. By mixing artificial sea and river water, the maximum output power density of 4.6W/m^2 could be obtained. In addition, by connecting 10 MXene membranes with opposite charges in series [Figure 16E], an output voltage of 1.66 V was obtained, which can supply power to electronic equipment directly. Figure 16F shows a numerical simulation diagram of the ion concentration distribution of cations (C_p) and anions (C_n) in nanofluidic

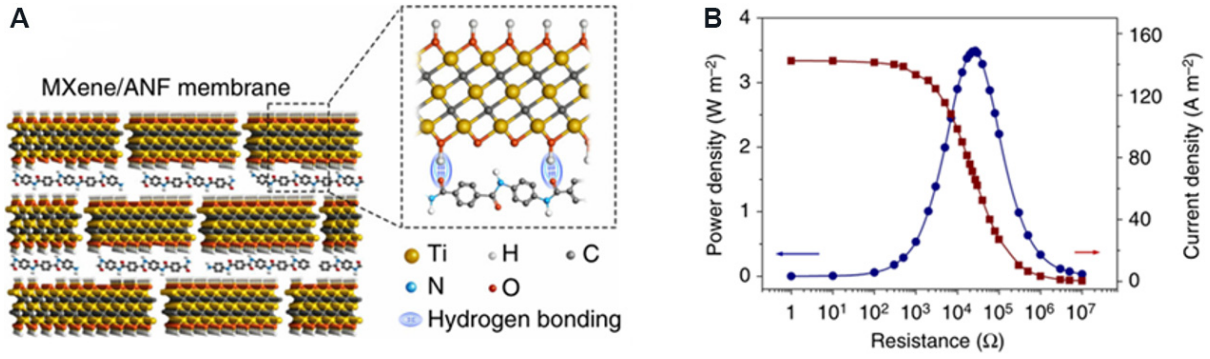

Figure 14. Schematic and electrical performance diagrams of MXene/ANF composite membrane. (A) Schematic diagram of composite membrane with CNFs intercalated between the layers of the MXene. (B) Electrical performance diagram of composite membrane, in which the power density increases at first and then decreases with increasing external resistance and the current density decreases with increasing external resistance. Figures reproduced with permission from Zhang *et al.*[27] (Copyright © 2019 Nature). ANF: Aramid nanofibers; CNFs cellulose nanofibers.

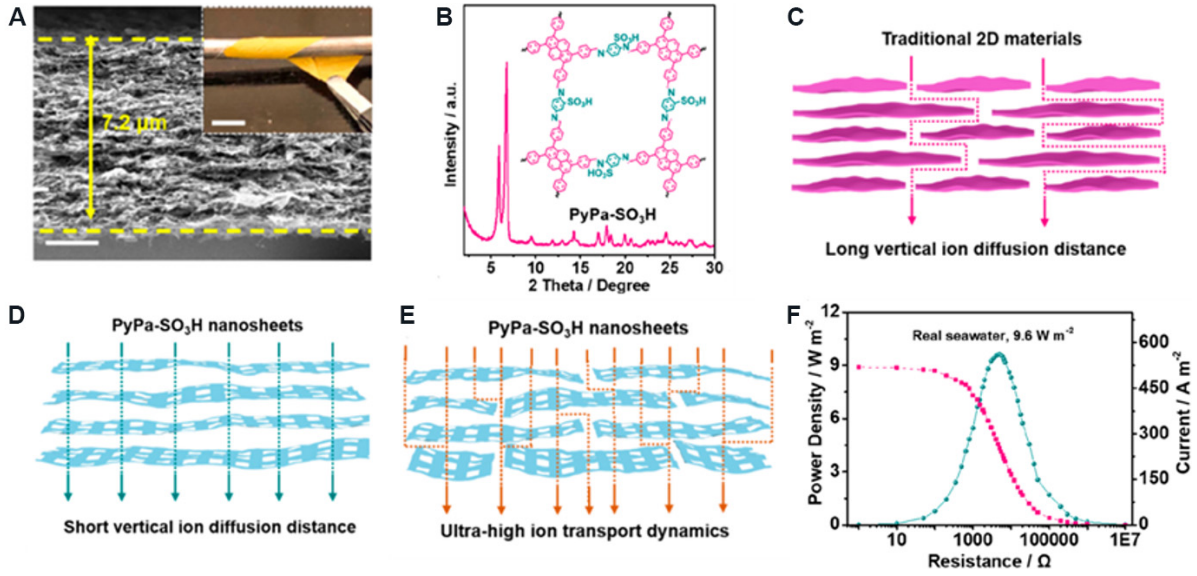

Figure 15. Structural and performance diagrams of PyPa-SO_3H/SANF composite membrane. (A) SEM image of PyPa-SO_3H/SANF composite membrane (scale: 200 nm). The illustration shows that the membrane has excellent flexibility (scale: 1 cm). (B) X-ray diffraction pattern of PyPa-SO_3H/SANF composite membrane. (C) Ion transport in traditional 2D nanofluidic membranes. (D) Vertical transport of ions through 1D nanochannels. (E) Horizontal and vertical transport of ions in PyPa-SO_3H/SANF composite membrane. (F) Variation of output power density and current of PyPa-SO_3H/SANF composite membrane with applied resistance. Figures reproduced with permission from Man *et al.*[54] (Copyright © 2021 American Chemical Society).

channels with different pore sizes. The numerical simulation results show that the small aperture nanochannels have excellent ion selectivity. This phenomenon is because the small aperture nanochannels can be completely covered by the EDL, while the large aperture nanochannels cannot be completely overlapped by the EDL, which leads to the deterioration of ion selectivity. Therefore, small aperture channels are conducive for reducing the influence of common ions into the channels and improving the energy conversion ability.

The energy output of a concentration cell can be regulated by an external field. Our team designed a temperature-controlled 2D nanofluidic membrane composed of functional MMT lamellae to realize the

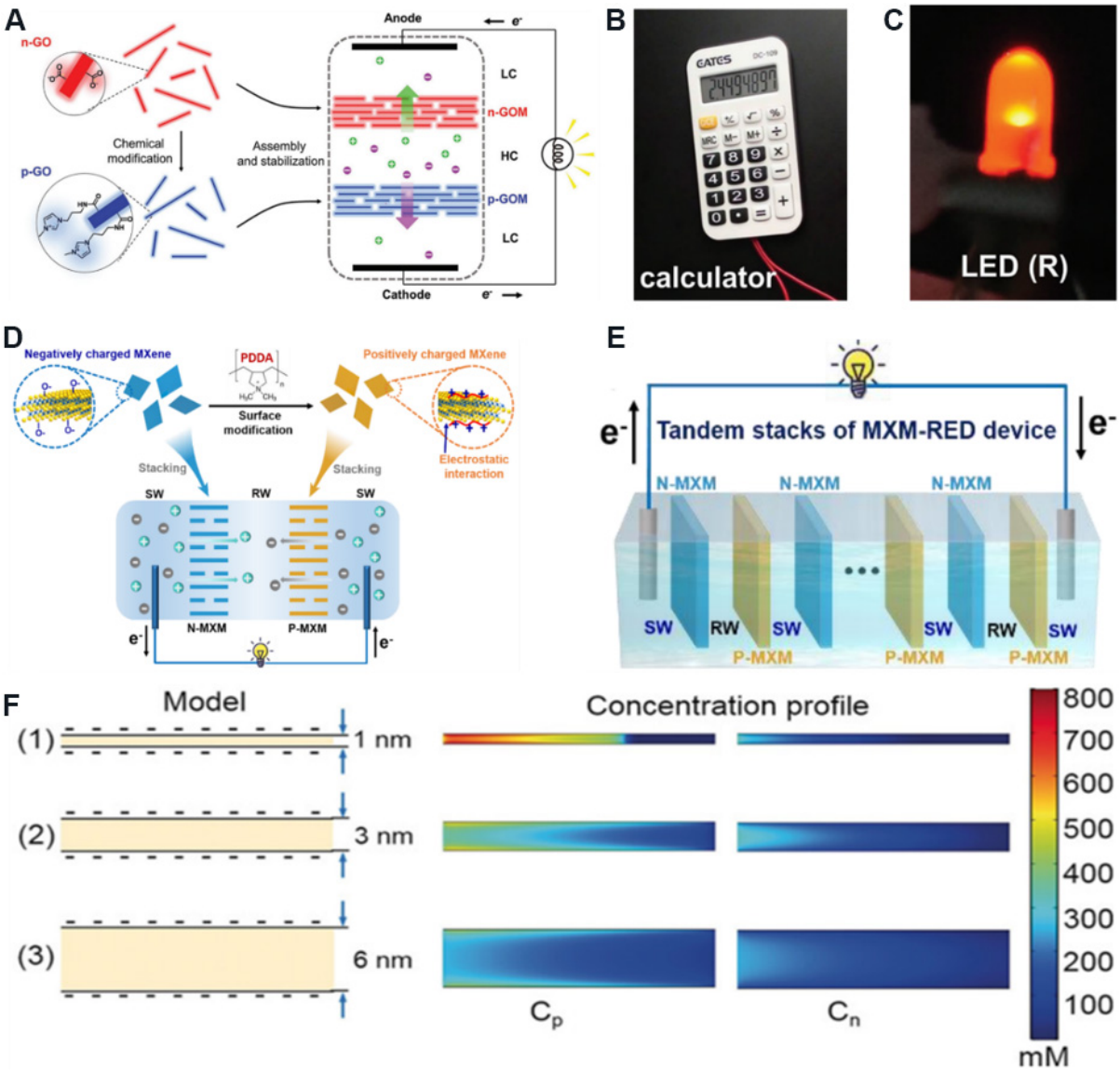

Figure 16. Schematic and numerical simulation diagrams of concentration cells based on 2D membranes with opposite charges in series. (A) Schematic diagram of concentration cell based on oppositely charged GO membranes. Concentration cell supplying power to (B) an electronic calculator and (C) a light-emitting diode. Figures reproduced with permission from Ji *et al.*[50] (Copyright © 2017 Wiley). (D) Schematic diagram of concentration cell based on oppositely charged MXene membranes. (E) Concentration cell based on multiple MXene membranes with opposite charges in series (RW is river water and SW is seawater). (F) Numerical simulation of ion concentration distribution of cations (C_p) and anions (C_n) in nanofluidic channels with different pore sizes. Figures reproduced with permission from Ding *et al.*[49] (Copyright © 2020 Wiley).

controllable energy output of the concentration cell [Figure 17A][52]. The membrane integrates two functional parts. The first is polyacrylic acid, which produces a high density of negative charge on the surface of the nanochannels to obtain excellent cationic selectivity. The other is dioctadecyl dimethyl ammonium bromide (DODAB), with a phase transition temperature of ~45 °C. The configuration transition of DODAB between different temperatures is helpful for the cation gating behavior. Figure 17B shows the I-V characteristic curve of the concentration cell at a 1000 times salinity gradient. The current output of the concentration cell is improved at 60 °C. In the cycles of alternating temperature switching shown in Figure 17C, the change in short-circuit current (I_{sc}) expresses ideal reversibility and stability.

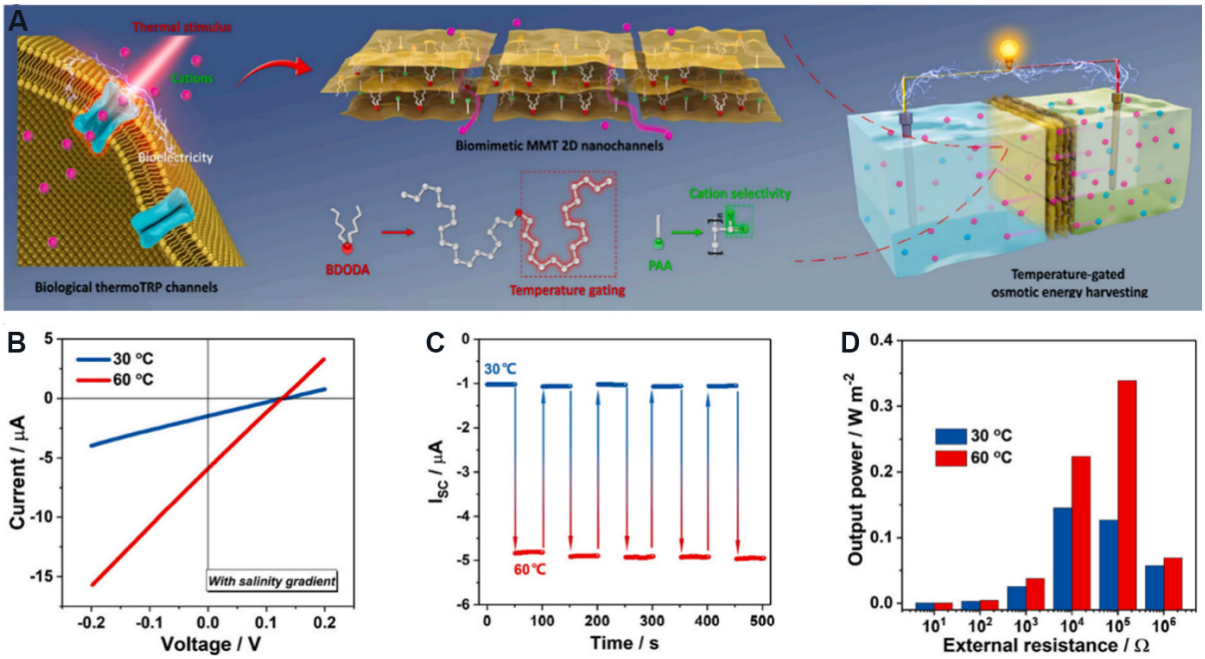

Figure 17. Schematic and performance diagrams of biomimetic temperature-controlled concentration cell based on MMT. (A) Schematic diagram of concentration cell. (B) I-V characteristic curve at a 1000 times salinity gradient. (C) I_{SC} variation under cycles of the alternating temperature switching. (D) Output power density at different temperatures and external resistors. Figures reproduced with permission from Wu *et al.*[52] (Copyright © 2020 Elsevier). MMT: Montmorillonite.

Figure 17D shows the output power density at different temperatures and external resistors. As the temperature increases from 30 to 60 °C, the output power density increases with a peak value of 0.34 W/m^2. Based on cation selectivity and temperature control of ion transport, concentration cells can adjust the energy output reversibly and stably through the alternating change of temperature, which provides the possibility for the design of intelligent concentration cells.

Current research concerning concentration cells based on 2D nanofluidic membranes is mainly focused on the horizontal transmembrane transport of ions. 2D membranes with vertical ion transport can also be used for osmotic power generation. Zhang *et al.*[125] reported a kind of vertical ion transport graphene oxide membrane (V-GO) with high ion selectivity and ultrafast ion transport. The ion transport capacity of V-GO is much higher than that of the horizontal ion transport graphene oxide membrane (H-GO). This is due to the different transport paths of ions in H-GO and V-GO. After entering H-GO, the ions take a zigzag trajectory to pass through the nanochannels, while ions travel in a straight line through V-GO, which effectively increases the ion transport rates. In addition, the geometry of V-GO provides more entrances for ions to enter the nanochannels, thereby allowing ions to enter the internal channels faster [Figure 18A]. The differences in ionic conductivity [Figure 18B] and ion mobility [Figure 18C] between V-GO and H-GO indicate the ultrafast ion transport ability of V-GO. Figure 18D shows the output current density of concentration cells based on V-GO or H-GO in different concentrations of electrolyte. The high current output of concentration cells based on V-GO certifies its excellent ion selectivity. Through the mixing of artificial sea and river water, the output power density of concentration cells based on V-GO can reach 10.6 W/m^2. The study of V-GO contributes to the practical application of osmotic energy and brings a novel design strategy for 2D nanofluidic membranes.

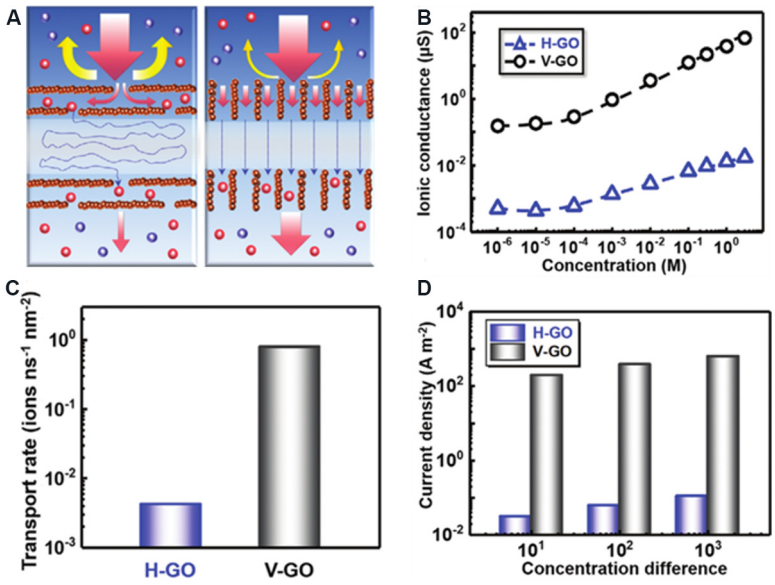

Figure 18. Schematic diagram of ion transport and performance diagram of H-GO and V-GO. (A) Comparison of ion transport paths between H-GO and V-GO. (B) Ionic conductivity of H-GO and V-GO in different concentrations of electrolyte. (C) Ion mobility of H-GO and V-GO. (D) Current density of H-GO and V-GO in different concentrations of electrolyte. Figures reproduced with permission from Zhang *et al.*[125] (Copyright © 2020 Wiley).

However, current reports on concentration cells are mainly focused on improving the performance of the membrane and the use of different concentrations of salt solutions, thereby ignoring the utilization of other solutions. Liu *et al.*[126] used HCl and KOH solutions to further explore the power generation performance of MXene membranes. The MXene membrane is placed between the two-chamber electrochemical cell containing the same concentration of HCl and KOH solutions. In the process of energy conversion, H^+ and K^+ can pass through the nanochannels of the MXene membrane. The ion mobility of H^+ is one order of magnitude higher than that of K^+, so the amount of H^+ passing through the membrane is much larger than that of K^+, which can induce the migration of net cations from the HCl side to the KOH side to form a directional cation current. In addition, when H^+ passes through the nanochannels of the MXene membrane and meets OH^-, an acid-base neutralization reaction occurs immediately and H^+ is consumed, which leads to the continuous migration of H^+ and efficient energy conversion. Figure 19A shows the variation of the open circuit voltage (V_{oc}) and short circuit current (I_{sc}) of the acid-base electrochemical cell with the acid-base concentration. I_{sc} and V_{oc} gradually increased with increasing acid and alkali concentrations. Figure 19B describes the output current and power densities of the acid-base electrochemical cell under different load resistances. The current density decreases with increasing load resistance and the power density increases at first and then decreases with increasing load resistance. When the concentrations of HCl and KOH are 0.01, 0.1 and 1 M, the maximum output power densities are 0.08, 1.14 and 7.89 W/m^2, respectively. This study provides a new strategy for research into the power generation of 2D nanofluidic membranes, and it is therefore important to investigate its potential applications in extreme environments.

In addition, other types of 2D nanofluidic membranes also have excellent properties and can be used as ion selective exchange membranes for concentration cells. Zhu *et al.*[117] prepared high-strength 2D MoS_2 composite membranes by combining chemically stripped MoS_2 nanosheets and CNFs. Due to the introduction of CNFs as enhancers, the composite membranes have high ionic conductivity and excellent mechanical properties. When artificial river and seawater are mixed, the output power density reaches 5.2 W/m^2. Xin *et al.*[127] prepared a 2D nanofluidic composite membrane with an asymmetric structure and

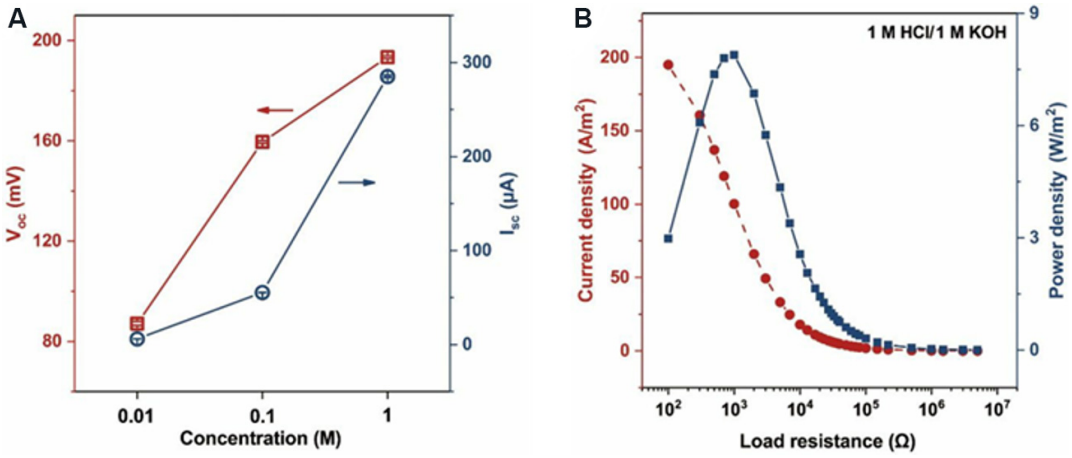

Figure 19. Performance diagram of electrochemical cell based on acid-base neutralization reaction. (A) V_{oc} and I_{sc} at different acid-base concentrations. (B) Output current and power densities under different load resistors. Figures reproduced with permission from Liu *et al.*[126] (Copyright © 2020 American Chemical Society).

charge polarity using SNF and anodic aluminum oxide (AAO) membranes [Figure 20A and B]. The SNF membrane contains nanochannels that dominate ion transport. The AAO membrane serves as a supporting substrate, providing adjustable channels and amphoteric groups. The output power density of the AAO/SNF composite membrane can reach 2.86 W/m² at a 50 times concentration gradient. Zhang *et al.*[128] prepared a black phosphorus (BP) membrane by assembling exfoliated BP nanosheets and explored the effect of oxidation of BP on the osmotic energy conversion of the BP membrane. The experimental results show that the coexistence of oxygen and water can accelerate the oxidation of BP and form phosphorus oxide compounds with different valence states that are correlated with the concentration of oxygen. These compounds can be used as charged sites in electrolyte solutions to accelerate ion transport and energy conversion, as shown in Figure 20C. In the process of energy conversion, high valence phosphorus oxide compounds provide more negative charge than low valence phosphorus oxide compounds and increase the power density from 0.5 to 1.6 W/m² (compared with the original BP membrane).

Li *et al.*[129] prepared a 2D nanofluidic composite membrane taking advantage of polystyrene sulfonate (PSS)/MOF composites and AAO. By adjusting the content of PSS in the composite membrane, the membrane exhibits excellent cationic selectivity. When artificial river and seawater are mixed, an output power density of 2.87 W/m² is acquired. However, there are few applications of MOF-based 2D nanofluidic membranes for osmotic energy conversion. Considering the porous structure of MOFs, it is possible to achieve ultrahigh ion transport similar to COFs for the construction of efficient concentration cells. Xiao *et al.*[130] fabricated an ultrathin free-standing carbon nitride membrane with excellent ion transport characteristics by chemical vapor deposition for salinity gradient energy conversion. An output power density of 0.21 W/m² was obtained under a 1000-fold salinity gradient. Gao *et al.*[131] fabricated a graphitic carbon nitride (g-C_3N_4)/CNF composite membrane [Figure 20D] by vacuum filtration to improve the output power density. The increased charge density imparted by the surface groups of CNFs facilitates the ion diffusion through the nanochannels among the layers of the g-C_3N_4/CNF composite membrane [Figure 20E]. Furthermore, the addition of CNFs greatly benefits the exfoliation of g-C_3N_4 nanosheets and enhances the mechanical properties of the composite membrane due to the strong hydrogen bonding formed between the -NH_2 or -NH groups in g-C_3N_4 nanosheets and the -OH or -COOH functional groups of CNFs. The output power density of 0.15 W/m² was obtained at a 1000-fold salinity gradient.

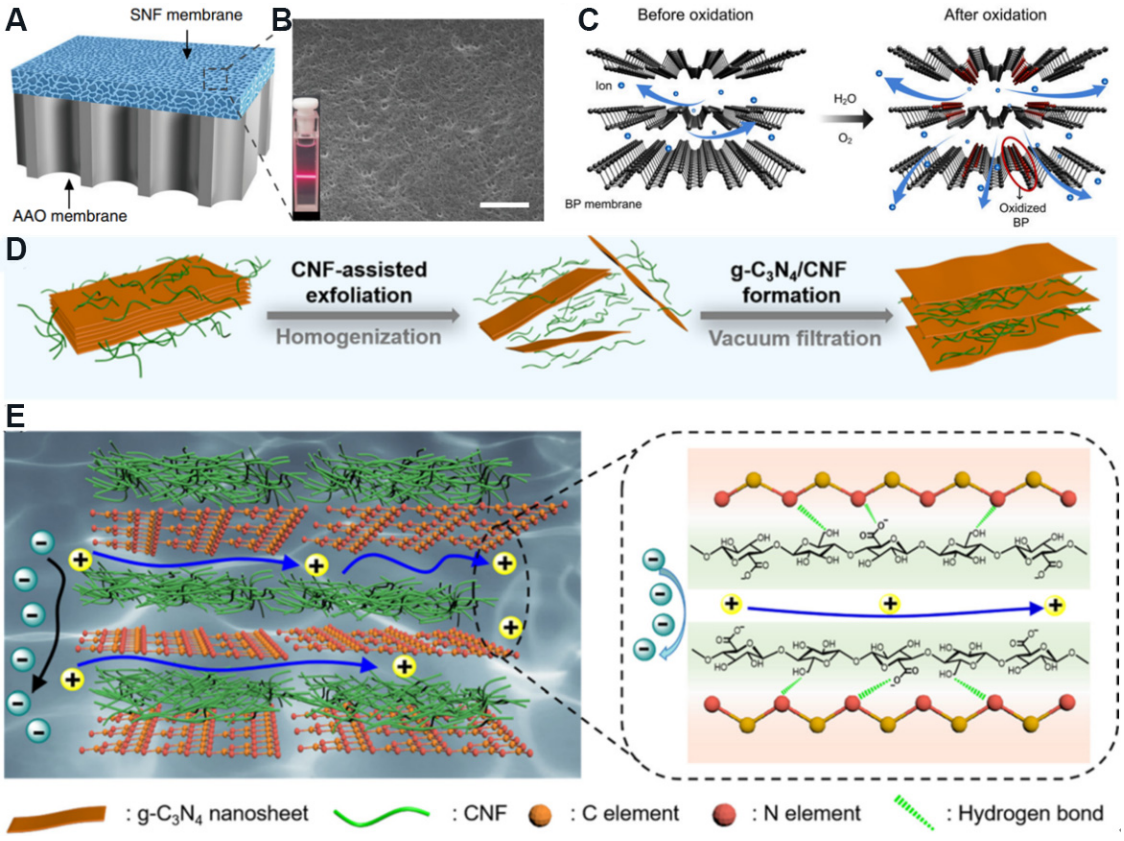

Figure 20. Schematic diagram of other 2D nanofluidic membranes. (A) AAO/SNF composite membrane. (B) SEM diagram of SNF membrane surface. Inset illustrates Tyndall light scattering effect of SNF solution. Figures reproduced with permission from Xin *et al.*[127] (Copyright © 2019 Nature). (C) Transport of ions across membrane before and after the oxidation of BP membrane (functional phosphorus compounds marked in red circle). Figure reproduced with permission from Zhang *et al.*[128] (Copyright © 2020 National Academy of Sciences). (D) Fabrication process of g-C_3N_4/CNF composite membrane. (E) Schematic diagram of selective ion transport in g-C_3N_4/CNF composite membrane. Figures reproduced with permission from Gao *et al.*[131] (Copyright © 2022 Elsevier). AAO: Anodic aluminum oxide; SNF: silk nanofiber; BP: black phosphorus; CNF: cellulose nanofiber.

The applications of salinity gradient-driven 2D nanofluidic generators are summarized in Table 2. The maximum power density that can be obtained by a concentration cell is generally several W/m^2, which increases with increasing concentration gradient. In addition, the output power density normally decreases with increasing membrane thickness. This is because the thicker the membrane, the greater the resistance, resulting in an increase in the internal resistance of the concentration cell system. Therefore, ultrathin nanofluidic membranes are ideal for constructing high-performance concentration cells. Furthermore, the membrane area has a certain effect on the output power. For 2D nanofluidic membranes of the same system, the smaller the membrane area, the higher the output power. However, the principle has not been studied, which is a point that should be paid attention to in future research of concentration cells.

Pressure-driven 2D nanofluidic generators

Working principle

Ion-selective 2D nanofluidic membranes are installed between a two-chamber electrochemical cell filled with the same solution and gas (such as nitrogen) is injected into one side of the electrochemical cell to provide pressure to push the liquid and ions to flow across the membrane. When the pressure reaches a certain limit, an electric current can be generated. Driven by pressure, the ions in the solution pass through the nanochannels in an almost unipolar manner. Combined with the electrostatic interaction, the common

Table 2. Summary of applications of salinity gradient-driven 2D nanofluidic generators

2D membranes	Thickness (μm)	Area (mm^2)	Concentration gradient (multiple)	Maximum output power density (W/m^2)	Ref.
GO/CNF	9	-	50	4.19	[124]
GO/SNF/GO	5	0.03	50	5.07	[48]
V-GO	350	0.00355	50	10.6	[125]
RKM	25	0.2	100	0.18	[122]
MMT (30 °C)	70	0.785	1000	0.15	[52]
MXene	2.7	0.0163	1000	21	[123]
MXene/ANF	4.5	0.03	150	3.7	[27]
SNF/AAO	65	0.03	50	2.86	[127]
BP	8	0.03	50	1.6	[128]
COF/ANF	7.2	20.74	150	9.6	[54]
C_3N_4	0.25	-	1000	0.21	[130]
g-C_3N_4/CNF	-	-	1000	1.4	[131]

GO: Graphene oxide; CNF: cellulose nanofiber; ANF: aramid nanofibers; AAO: anodic aluminum oxide; SNF: silk nanofiber; BP: black phosphorus; COF: covalent organic framework.

ions in the nanochannels are completely repelled from the layered nanochannels, and the counter ions become single carriers to form net ion currents [Figure 21][132].

Application examples

In order to harvest blue energy, Wu *et al.*[124] prepared a graphene hydrogel membrane (GHM) using a dispersed reduced graphene colloid solution by vacuum filtration and studied its pressure-driven power generation capacity. The GHM is installed between a two-chamber electrochemical cell, and nitrogen pressure is applied at one side of the electrochemical cell to promote the liquid to flow across the membrane. Above a threshold pressure of ~2 kPa, the ion current of synchronous flow can be observed, indicating that the hydraulic energy is converted into electric energy. When the pressure gradient is less than 2 kPa, the pressure-induced ion current cannot be observed. This is due to the hydrophobic property of the graphene membrane, which requires a strong enough mechanical force to overcome the resistance of the hydrogel network. However, when the pressure gradient is greater than 10 kPa, the GHM is prone to mechanical fracture. Therefore, an appropriate pressure value is needed to obtain the best current output. For example, when the pressure of 5 kPa is applied, a continuous current output of 2.23 ± 0.26 nA can be obtained in a 0.1 M NaCl solution. In addition, the team injected gas from different sides of the electrochemical cell and studied the bidirectional response performance of the ion current of the electrochemical cell driven by the pressure [Figure 22A].

Figure 22B and C show the variation of bidirectional ion current with time when a reverse pressure (5 kPa for 2 s) is applied. Once the electrolyte flows in the opposite direction, the resulting ionic current also reverses. With the input of gas, the ion current increases sharply to the peak value within 1 s and then decreases with decreasing gas pressure. However, the duration of the electrical signal is much longer than that of the gas pressure due to the fact that the gas pressure on both sides of the membrane is still unbalanced for a short time after the pressure is stopped, so the decrease of ion current lags behind the decrease in pressure. Cheng *et al.*[122] prepared an RKM for research on pressure-driven energy conversion. Driven by the transmembrane hydraulic flow, a considerable flowing ion current was observed. When the flow rate is 5 mL/min, the flowing current is close to several hundred nA in a 0.01 M KCl solution. The flowing current generated is generally linear with the flow rate.

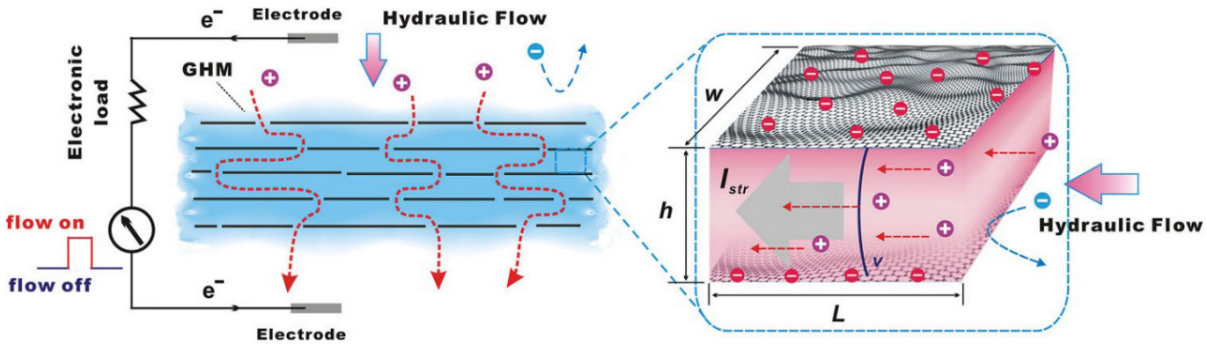

Figure 21. Working principle of pressure-driven generator based on 2D nanofluidics. Figure reproduced with permission from Guo *et al.*[132] (Copyright © 2013 Wiley).

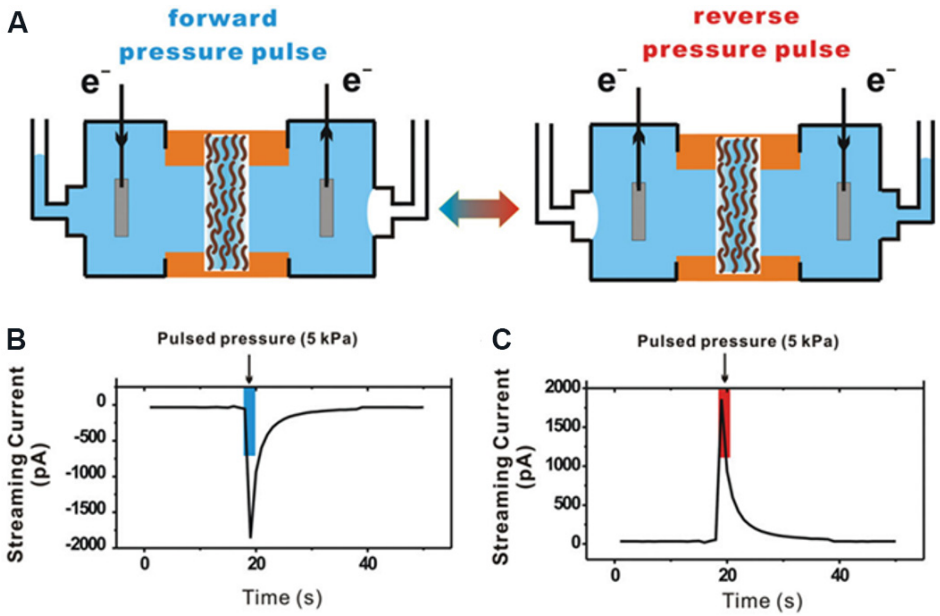

Figure 22. Schematic and performance diagrams of pressure-driven electrochemical cell based on GHM. (A) Injection of gas on different sides of electrochemical cell. Change in flow current when (B) forward and (C) reverse pressure are applied to the electrochemical cell. Figures reproduced with permission from Guo *et al.*[132] (Copyright © 2013 Wiley). GHM: Graphene hydrogel membrane.

Yang *et al.*[133] fabricated 2D MXene nanofluidics membranes by vacuum suction filtration for the construction of pressure-driven generators. A streaming current of 26 nA was obtained under a pressure gradient of 5 kPa. Qu *et al.*[134] reported vertically-oriented MXene membranes (VMMs) with ultrafast ion transport, as well as high ion selectivity for pressure-driven power generation [Figure 23A]. Compared with horizontally stacked MXene membranes (HMMs), the ultrafast ion transport in VMMs originates from the evidently short migration paths and the low energy loss during ionic migration [Figure 23B]. In addition, the ionic conductance in VMMs is greater than that in HMMs, indicating that ions transport faster and the flow current density is higher in VMMs [Figure 23C and D]. At a pressure gradient of 5 kPa, a flowing current output of 50 nA can be obtained for a pressure-driven generator based on VMMs.

To expand the practical application range of pressure-driven nanofluidic generators, more stable membrane materials must be developed. Boron nitride (BN) nanosheets are 2D layered nanomaterials that are

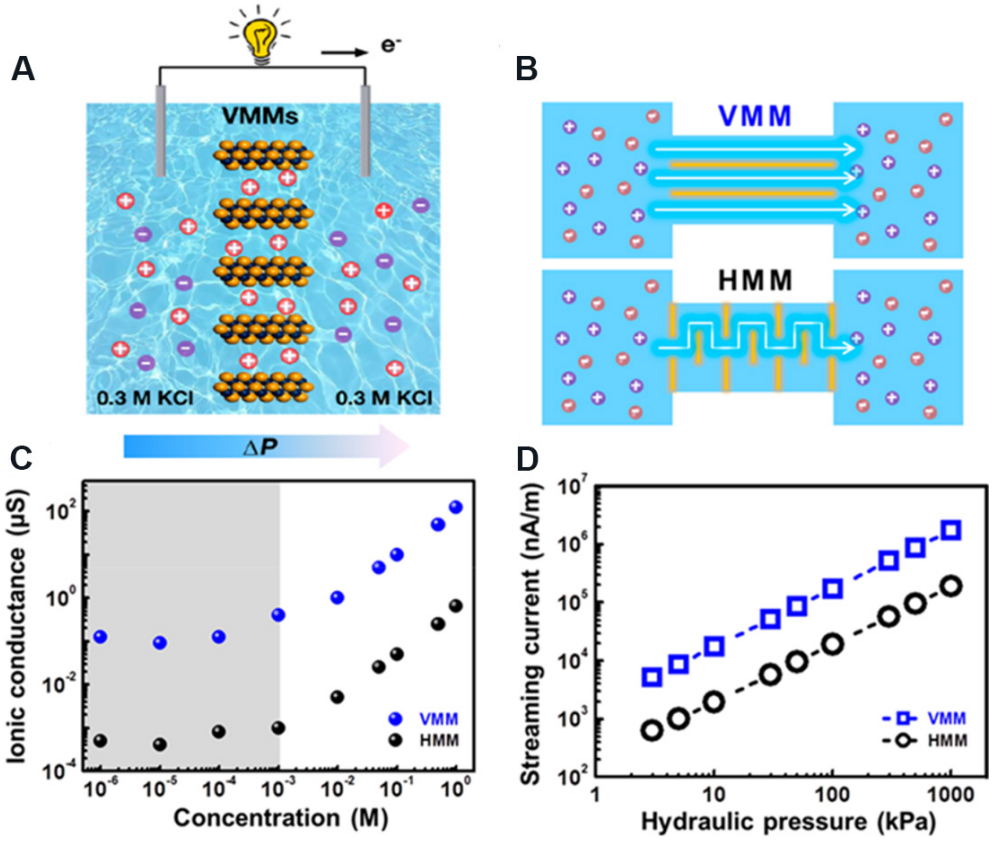

Figure 23. Schematic and performance diagrams of pressure-driven generator based on VMMs. (A) Schematic diagram of pressure-driven generator based on VMMs. (B) Ion transport in HMMs and VMMs. (C) Ionic conductance of VMMs and HMMs. (D) Streaming currents growing linearly with hydraulic pressure. Figures reproduced with permission from Qu *et al.*[134] (Copyright © 2020 American Chemical Society). VMMs: Vertically-oriented MXene membranes; HMMs: horizontally stacked MXene membranes.

composed of boron and nitrogen atoms arranged in a hexagonal plane similar to the carbon atoms in graphene. BN 2D nanofluidic membranes provide plentiful nanochannels and are ideal materials for the construction of pressure-driven nanofluidic generators. Qin *et al.*[135] prepared a BN membrane [Figure 24A and B] for pressure-driven power generation. In the experiment, the BN membrane with an area of 5 mm^2 was installed between a sealed two-chamber electrochemical cell filled with electrolytes, as shown in Figure 24C. When a nitrogen pressure of 5 kPa was applied, an output current of 12.1 ± 1.5 nA and a maximum output power of 0.64 mW/m^2 were produced in a 0.1 M NaCl solution. As the ion concentration increases from 0.001 to 0.01 M, the current response increases significantly. However, when the ion concentration further increases to 0.1 M, the current response remains relatively stable. This demonstrates that there is an upper limit for the selective transport of ions through the membrane under external pressure. In addition, when alternating forward and reverse pressures are applied, a bidirectional current response can be observed, meaning that the device can operate in both directions. This work provided new insights into alternating current output from blue energy harvesting systems.

The applications of the reported pressure-driven generators based on 2D nanofluidics are summarized in Table 3. The maximum power density that can be obtained from pressure-driven power generation is several mW/m^2, which is several orders of magnitude lower than that of concentration cells. The different concentration of the electrolyte solution also affects the power density. In addition, the output power density of pressure-driven power generation also decreases with increasing membrane thickness, which can

Table 3. Summary of applications of pressure-driven generators based on 2D nanofluidics

2D membranes	Thickness (μm)	Area (mm^2)	Pressure gradient (kPa)	Streaming current (nA)	Output power density (mW/m^2)	Ref.
GHM	-	3	5	2.23	-	[132]
MXene	0.11	19.6	5	26	0.00029	[133]
VMMs	320	0.04	5	50	25	[134]
BN	22	5	5	12.1	0.64	[135]

GHM: Graphene hydrogel membrane; VMMs: vertically-oriented MXene membranes; BN: boron nitride.

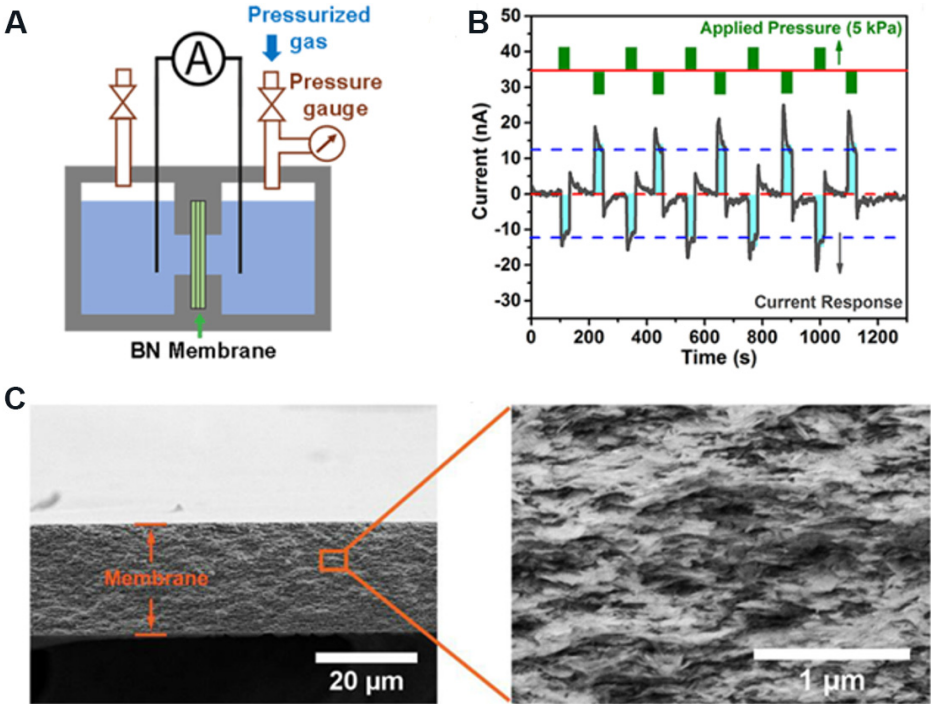

Figure 24. Schematic and performance diagrams of pressure-driven electrochemical cell. (A) Pressure-driven electrochemical cell. (B) Current response under alternating pressure in different directions, indicating that the membrane can work when pressure is applied in different directions. (C) SEM image of the cross section of a BN membrane with a thickness of 22 μm. The inset shows the layered structure formed by the stacking of BN nanosheets. Figures reproduced with permission from Qin *et al.*[135] (Copyright © 2018 Elsevier). BN: Boron nitride.

be attributed to the corresponding high resistance and long transport path of ions through membranes. Since there are few related kinds of research on pressure-driven generators based on 2D nanofluids, many performance parameters and data need to be further studied.

PROSPECT AND CHALLENGES

Although 2D nanofluidics have demonstrated promising applications in blue energy harvesting, significant progress is still required to push this technology into practical applications. Thus, several prospects and challenges are proposed and discussed to provide directions for further studies.

Comparison of generators based on 2D nanofluidics with traditional and emerging power generators for blue energy harvesting

Currently, there are a variety of conventional techniques for harvesting blue energy. For example, Open Hydro in Ireland has designed seabed turbines to harvest tidal energy[136]. The British company Pelamis has

designed a wave power generation device and realized grid-connected power generation. Although these traditional technologies have a certain industrial foundation and are used for commercialization, problems such as heavy equipment, high cost and complex technology still exist. Furthermore, devices based on conventional electromagnetic power generation techniques cannot harvest low-frequency energy (< 5 Hz) in the ocean[137]. Therefore, conventional blue energy harvesting devices exhibit unsatisfactory energy harvesting efficiency and high cost. In contrast, the generators based on 2D nanofluidics have simple power generation principles (e.g., primary battery principle), convenient equipment and low cost. The increasing maturity of membrane technology is also conducive to the further development of generators based on 2D nanofluids in blue energy harvesting.

New blue energy harvesting technologies, such as triboelectric nanogenerators (TENGs)[138], have also attracted extensive attention. TENGs can convert low-frequency and low-amplitude mechanical energy in the ocean into electrical energy, which is an important supplement to traditional techniques. For example, Lin *et al.*[139] used polydimethylsiloxane and polytetrafluoroethylene as hydrophobic and highly negative materials to design a TENG based on contact electrification. This new prototype TENG provided a peak power density of nearly 0.13 W/m^2. Wen *et al.*[140] invented a TENG that is based on a wavy structured Cu-Kapton-Cu film with a peak power density of 0.4 W/m^2. However, TENGs are susceptible to the intermittent power supply caused by environmental and climate change, which limits their practical application in stable power supplies. In addition, the output power density of TENGs is also lower than that of generators based on 2D nanofluidics. In contrast, generators based on 2D nanofluidics can harvest blue energy in a continuous and stable manner, which is conducive to providing relatively stable and sustainable all-weather power output. Thus, nanofluids have more significant advantages in continuous power supply and energy density.

Large-scale production of high-performance 2D nanofluidics

It is necessary to realize the large-scale production of high-performance 2D nanofluidic membranes to meet the requirements of practical applications. High-performance 2D nanofluidic membranes usually require high mechanical strength and excellent environmental tolerance to resist the performance decay and structural corrosion in seawater during long-term operation. In contrast, it is also important to reduce the fabrication cost of 2D membranes to achieve large-scale commercial production.

Among the widely studied materials for 2D nanofluidic membranes, inorganic materials, such as GO and MXenes, have abundant surface groups and large specific surface areas, which can be easily modified. The electrical properties of MXenes are excellent. However, the cost of inorganic materials is expensive, and their preparation process is complicated, so it is difficult to achieve large-scale production. Other clay-based inorganic materials, such as MMT, are low-cost and easy to prepare, which are expected to achieve large-scale and low-cost production. However, the low output power density of clay-based 2D nanofluidics is difficult to meet commercial standards due to poor electrical conductivity (high electrical resistance and low ionic conductivity affect ion transport). Complex materials, such as COFs and MOFs, have large specific surface areas, high porosity, regular pore structure and low density, and can be used to prepare 2D nanofluidic membranes with better performance for blue energy harvesting. However, these complex materials are difficult to prepare into continuous and dense self-supporting membranes with excellent mechanical properties. Polymer materials, such as sulfonated polyether ether ether ketone[141,142], have the advantages of high mechanical strength, corrosion resistance and effortless processing. The disadvantage of polymer membrane is that the 1D nanopore structure is uneven, resulting in poor ion flux and selectivity. As mentioned above, single-material membranes have limited performance. Therefore, composite membranes can be prepared by compounding different materials to improve the mechanical and electrical properties, such as COF/ANF and GO/CNF membranes. Furthermore, reducing the fabrication cost of GO,

MXenes and COF membranes or improving the output power density of clay-based membranes is the key to achieving low-cost and large-scale production.

Inconvenient integration and packaging of devices

Concentration cells based on 2D nanofluidic membranes also face considerable challenges in practical applications, such as the integration and packaging of devices. To prepare a portable concentration cell, 2D nanofluidic membranes, electrodes and sea and river water must be packaged in a device to prevent the interference of impurities and moisture in the air. Due to the concentration cell needing to hold a certain amount of sea and river water, the device packaging must select a suitable shell material to resist the corrosion of sea and river water and to prevent water leakage. Therefore, shell materials should possess favorable corrosion resistance and sealing, including new alloy and composite materials, which increase the cost accordingly. In contrast, the device will be greatly affected by the outside conditions, such as device inversion and vibration, which requires relative stability between the internal structures of the device, such as the fixation of electrodes and membranes. For concentration cells with multiple membranes in series, device packaging is more formidable. Moreover, the power generation conditions of concentration cells in most experiments are ideal, and there is almost no external interference in the laboratory. However, the long-term stability of concentration cells in practical use is difficult to guarantee.

Unsatisfactory energy density

Another challenge for the practical application of 2D nanofluidic membranes in blue energy harvesting is that the output power density is difficult to meet commercial standards. For practical applications, the power supply capacity of power generation devices is not sufficient to meet the needs of practical applications if there is no significant energy output. Furthermore, the advantages of osmotic power generation compared with other clean energy power generation technologies are not dominant; it is difficult to replace some traditional and new energy power generation technologies. Increasing the energy density by reducing the membrane resistance and connecting multiple membranes with opposite charges in series are feasible methods, but this puts forward higher requirements for correlation techniques.

In addition, the energy output of concentration cells is sustainable because cations continue to pass through the membrane and generate currents. Therefore, the flexibility of integrated cells in practical application is undesirable, and the power output cannot be controlled according to the actual demand. To achieve controllable energy output, it is necessary to prepare high-quality intelligent response membranes (e.g., temperature-gated MMT membranes) so that ion transport can be regulated by external stimuli.

CONCLUSIONS

In summary, the unique merits of 2D nanofluidics are crucial for the utilization of blue energy. This review has summarized the recent advances and progress in the applications of 2D nanofluidic membranes in effective blue energy harvesting. The principles and advantages of nanofluidic channels in regulating ion transport toward blue energy harvesting are discussed in detail. The prospects for real-world applications of 2D nanofluidic membranes in blue energy harvesting are also proposed, such as high-performance membranes for device integration and large-scale and low-cost membranes to meet the requirements of practical applications. Furthermore, the challenges faced by 2D nanofluidic membranes in device integration, energy output and stability are presented, thereby providing a novel strategy for the development of high-performance blue energy harvesting systems.

DECLARATIONS

Authors' contributions

Writing - original draft preparation: Xie L, Tang J
Investigation: Qin R
Writing - reviewing and Editing: Zhang Q, Wang H
Supervision: Liu J, Jin Y

Availability of data and materials

Not applicable.

Financial support and sponsorship

This work was supported by Natural Science Foundation of Beijing Municipality (No. 2212001), Beijing Nova Program (No. Z201100006820112) and National Natural Science Foundation of China (No. 62075002).

Conflicts of interest

All authors declared that there are no conflicts of interest.

Ethical approval and consent to participate

Not applicable.

Consent for publication

Not applicable.

REFERENCES

1. Zou C, Zhao Q, Zhang G, Xiong B. Energy revolution: from a fossil energy era to a new energy era. *Natural Gas Industry B* 2016;3:1-11. DOI
2. Sims R. Renewable energy: a response to climate change. *Solar Energy* 2004;76:9-17. DOI
3. Wang Z, Carriveau R, Ting DS, Xiong W, Wang Z. A review of marine renewable energy storage. *Int J Energy Res* 2018;43:6108-50. DOI
4. Opan M, Ünlü M, Özkale C, Çelik C, Saraç Hİ. Optimal energy production from wind and hydroelectric power plants. *Energ Source Part A* 2019;41:2219-32. DOI
5. Zhu X, Hao J, Bao B, et al. Unique ion rectification in hypersaline environment: a high-performance and sustainable power generator system. *Sci Adv* 2018;4:eaau1665. DOI PubMed PMC
6. Nijmeijer K, Metz S. Chapter 5 salinity gradient energy. *Sustainability Science and Engineering* 2010;2:95-139. DOI
7. Yip NY, Elimelech M. Thermodynamic and energy efficiency analysis of power generation from natural salinity gradients by pressure retarded osmosis. *Environ Sci Technol* 2012;46:5230-9. DOI PubMed
8. Economides MJ, Wood DA. The state of natural gas. *J Nat Gas Sci Eng* 2009;1:1-13. DOI
9. Aslam M, Masjuki H, Kalam M, Abdesselam H, Mahlia T, Amalina M. An experimental investigation of CNG as an alternative fuel for a retrofitted gasoline vehicle. *Fuel* 2006;85:717-24. DOI
10. Schaetzle O, Buisman CJ. Salinity gradient energy: current state and new trends. *Engineering* 2015;1:164-6. DOI
11. Avci AH, Tufa RA, Fontananova E, Di Profio G, Curcio E. Reverse Electrodialysis for energy production from natural river water and seawater. *Energy* 2018;165:512-21. DOI
12. Post JW, Hamelers HV, Buisman CJ. Energy recovery from controlled mixing salt and fresh water with a reverse electrodialysis system. *Environ Sci Technol* 2008;42:5785-90. DOI PubMed
13. Mei Y, Tang CY. Recent developments and future perspectives of reverse electrodialysis technology: a review. *Desalination* 2018;425:156-74. DOI
14. Talavera K, Nilius B, Voets T. Neuronal TRP channels: thermometers, pathfinders and life-savers. *Trends Neurosci* 2008;31:287-95. DOI PubMed
15. Xu J, Lavan DA. Designing artificial cells to harness the biological ion concentration gradient. *Nat Nanotechnol* 2008;3:666-70. DOI

PubMed PMC

16. Sparreboom W, van den Berg A, Eijkel JC. Principles and applications of nanofluidic transport. *Nat Nanotechnol* 2009;4:713-20. DOI PubMed
17. Zhu J, Wang L, Wang J, et al. Precisely tunable ion sieving with an Al_{13}-$Ti_3C_2T_x$ lamellar membrane by controlling interlayer spacing. *ACS Nano* 2020;14:15306-16. DOI PubMed
18. Peng Y, Li Y, Ban Y, Yang W. Two-dimensional metal-organic framework nanosheets for membrane-based gas separation. *Angew Chem* 2017;129:9889-93. DOI PubMed
19. Wang H, He S, Qin X, Li C, Li T. Interfacial engineering in metal-organic framework-based mixed matrix membranes using covalently grafted polyimide brushes. *J Am Chem Soc* 2018;140:17203-10. DOI PubMed
20. Ji YL, Gu BX, Xie SJ, et al. Superfast water transport zwitterionic polymeric nanofluidic membrane reinforced by metal-organic frameworks. *Adv Mater* 2021;33:e2102292. DOI PubMed
21. Luan P, Zhao Y, Li Q, et al. Compressible ionized natural 3D interconnected loofah membrane for salinity gradient power generation. *Small* 2022;18:e2104320. DOI PubMed
22. Zhang X, Wen Q, Wang L, et al. Asymmetric electrokinetic proton transport through 2D nanofluidic heterojunctions. *ACS Nano* 2019;13:4238-45. DOI PubMed
23. Zhang Q, Liu Q, Kang J, et al. Robust sandwich-structured nanofluidic diodes modulating ionic transport for an enhanced electrochromic performance. *Adv Sci (Weinh)* 2018;5:1800163. DOI PubMed PMC
24. Xiao K, Jiang L, Antonietti M. Ion transport in nanofluidic devices for energy harvesting. *Joule* 2019;3:2364-80. DOI
25. Xie G, Li P, Zhao Z, et al. Light- and electric-field-controlled wetting behavior in nanochannels for regulating nanoconfined mass transport. *J Am Chem Soc* 2018;140:4552-9. DOI PubMed
26. Guo W, Cao L, Xia J, et al. Energy harvesting with single-ion-selective nanopores: a concentration-gradient-driven nanofluidic power source. *Adv Funct Mater* 2010;20:1339-44. DOI
27. Zhang Z, Yang S, Zhang P, Zhang J, Chen G, Feng X. Mechanically strong MXene/Kevlar nanofiber composite membranes as high-performance nanofluidic osmotic power generators. *Nat Commun* 2019;10:2920. DOI PubMed PMC
28. Ding L, Li L, Liu Y, et al. Effective ion sieving with Ti3C2Tx MXene membranes for production of drinking water from seawater. *Nat Sustain* 2020;3:296-302. DOI
29. Zhang Q, Liu Z, Hou X, Fan X, Zhai J, Jiang L. Light-regulated ion transport through artificial ion channels based on TiO_2 nanotubular arrays. *Chem Commun (Camb)* 2012;48:5901-3. DOI PubMed
30. Zhang Q, Liu Z, Wang K, Zhai J. Organic/inorganic hybrid nanochannels based on Polypyrrole-embedded alumina nanopore arrays: pH- and light-modulated ion transport. *Adv Funct Mater* 2015;25:2091-8. DOI
31. Macha M, Marion S, Nandigana VVR, Radenovic A. 2D materials as an emerging platform for nanopore-based power generation. *Nat Rev Mater* 2019;4:588-605. DOI
32. Li R, Fan X, Liu Z, Zhai J. Smart Bioinspired nanochannels and their applications in energy-conversion systems. *Adv Mater* 2017;29:1702983. DOI PubMed
33. Liu P, Hou J, Zhang Y, Li L, Lu X, Tang Z. Two-dimensional material membranes for critical separations. *Inorg Chem Front* 2020;7:2560-81. DOI
34. Gao J, Feng Y, Guo W, Jiang L. Nanofluidics in two-dimensional layered materials: inspirations from nature. *Chem Soc Rev* 2017;46:5400-24. DOI PubMed
35. Koltonow AR, Huang J. IONIC TRANSPORT. Two-dimensional nanofluidics. *Science* 2016;351:1395-6. DOI PubMed
36. Schoch RB, Renaud P. Ion transport through nanoslits dominated by the effective surface charge. *Appl Phys Lett* 2005;86:253111. DOI
37. Zhang Q, Kang J, Xie Z, Diao X, Liu Z, Zhai J. Highly efficient gating of electrically actuated nanochannels for pulsatile drug delivery stemming from a reversible wettability switch. *Adv Mater* 2018;30:1703323. DOI PubMed
38. Hao Z, Zhou T, Xiao T, et al. Electrochromic nanochannels for visual nanofluidic manipulation in integrated ionic circuits. *ACS Appl Mater Interfaces* 2020;12:57314-21. DOI PubMed
39. Cao L, Xiao F, Feng Y, et al. Anomalous channel-length dependence in nanofluidic osmotic energy conversion. *Adv Funct Mater* 2017;27:1604302. DOI
40. Asghar W, Ilyas A, Billo JA, Iqbal SM. Shrinking of solid-state nanopores by direct thermal heating. *Nanoscale Res Lett* 2011;6:372. DOI PubMed PMC
41. Ho C, Qiao R, Heng JB, et al. Electrolytic transport through a synthetic nanometer-diameter pore. *Proc Natl Acad Sci U S A* 2005;102:10445-50. DOI PubMed PMC
42. Apel P. Track etching technique in membrane technology. *Radiation Measurements* 2001;34:559-66. DOI
43. Zhang B, Zhang Y, White HS. The nanopore electrode. *Anal Chem* 2004;76:6229-38. DOI PubMed
44. Martin CR, Nishizawa M, Jirage K, Kang M. Investigations of the transport properties of gold nanotubule membranes. *J Phys Chem B* 2001;105:1925-34. DOI
45. Karahan HE, Goh K, Zhang CJ, et al. MXene materials for designing advanced separation membranes. *Adv Mater* 2020;32:e1906697. DOI PubMed
46. Childs RF, Weng J, Kim M, Dickson JM. Formation of pore-filled microfiltration membranes using a combination of modified interfacial polymerization and grafting. *J Polym Sci A Polym Chem* 2002;40:242-50. DOI

47. Dreyer DR, Todd AD, Bielawski CW. Harnessing the chemistry of graphene oxide. *Chem Soc Rev* 2014;43:5288-301. DOI PubMed
48. Xin W, Xiao H, Kong XY, et al. Biomimetic nacre-like silk-crosslinked membranes for osmotic energy harvesting. *ACS Nano* 2020;14:9701-10. DOI PubMed
49. Ding L, Xiao D, Lu Z, et al. Oppositely charged $Ti_3C_2T_x$ MXene membranes with 2D nanofluidic channels for osmotic energy harvesting. *Angew Chem* 2020;132:8798-804. DOI
50. Ji J, Kang Q, Zhou Y, et al. Osmotic power generation with positively and negatively charged 2D nanofluidic membrane pairs. *Adv Funct Mater* 2017;27:1603623. DOI
51. Chen J, Xin W, Chen W, et al. Biomimetic nanocomposite membranes with ultrahigh ion selectivity for osmotic power conversion. *ACS Cent Sci* 2021;7:1486-92. DOI PubMed PMC
52. Wu C, Xiao T, Tang J, et al. Biomimetic temperature-gated 2D cationic nanochannels for controllable osmotic power harvesting. *Nano Energy* 2020;76:105113. DOI
53. Liu J, Wang N, Yu LJ, et al. Bioinspired graphene membrane with temperature tunable channels for water gating and molecular separation. *Nat Commun* 2017;8:2011. DOI PubMed PMC
54. Man Z, Safaei J, Zhang Z, et al. Serosa-mimetic nanoarchitecture membranes for highly efficient osmotic energy generation. *J Am Chem Soc* 2021;143:16206-16. DOI PubMed
55. Wang Y, Wu N, Wang Y, et al. Graphite phase carbon nitride based membrane for selective permeation. *Nat Commun* 2019;10:2500. DOI PubMed PMC
56. Huang H, Song Z, Wei N, et al. Ultrafast viscous water flow through nanostrand-channelled graphene oxide membranes. *Nat Commun* 2013;4:2979. DOI PubMed
57. Abraham J, Vasu KS, Williams CD, et al. Tunable sieving of ions using graphene oxide membranes. *Nat Nanotechnol* 2017;12:546-50. DOI PubMed
58. Ma M, Tocci G, Michaelides A, Aeppli G. Fast diffusion of water nanodroplets on graphene. *Nat Mater* 2016;15:66-71. DOI PubMed
59. Hu M, Mi B. Enabling graphene oxide nanosheets as water separation membranes. *Environ Sci Technol* 2013;47:3715-23. DOI PubMed
60. Joshi RK, Carbone P, Wang FC, et al. Precise and ultrafast molecular sieving through graphene oxide membranes. *Science* 2014;343:752-4. DOI PubMed
61. Yin Z, Lu Z, Xu Y, et al. Supported MXene/GO composite membranes with suppressed swelling for metal ion sieving. *Membranes (Basel)* 2021;11:621. DOI PubMed PMC
62. Guo W, Tian Y, Jiang L. Asymmetric ion transport through ion-channel-mimetic solid-state nanopores. *Acc Chem Res* 2013;46:2834-46. DOI PubMed
63. Bohinc K, Kralj-iglič V, Iglič A. Thickness of electrical double layer. Effect of ion size. *Electrochimica Acta* 2001;46:3033-40. DOI
64. Stein D, Kruithof M, Dekker C. Surface-charge-governed ion transport in nanofluidic channels. *Phys Rev Lett* 2004;93:035901. DOI PubMed
65. Hao Q, Zhao C, Sun B, et al. Confined synthesis of two-dimensional covalent organic framework thin films within superspreading water layer. *J Am Chem Soc* 2018;140:12152-8. DOI PubMed
66. Liu Y, Wei Y, Liu M, et al. Face-to-face growth of wafer-scale 2D semiconducting MOF films on dielectric substrates. *Adv Mater* 2021;33:e2007741. DOI PubMed
67. Wang L, Boutilier MSH, Kidambi PR, Jang D, Hadjiconstantinou NG, Karnik R. Fundamental transport mechanisms, fabrication and potential applications of nanoporous atomically thin membranes. *Nat Nanotechnol* 2017;12:509-22. DOI PubMed
68. Ren CE, Alhabeb M, Byles BW, et al. Voltage-gated ions sieving through 2D MXene $Ti_3C_2T_x$ membranes. *ACS Appl Nano Mater* 2018;1:3644-52. DOI
69. Kim KS, Zhao Y, Jang H, et al. Large-scale pattern growth of graphene films for stretchable transparent electrodes. *Nature* 2009;457:706-10. DOI PubMed
70. Shams SS, Zhang R, Zhu J. Graphene synthesis: a review. *Mater Sci Pol* 2015;33:566-78. DOI
71. Li X, Cai W, An J, et al. Large-area synthesis of high-quality and uniform graphene films on copper foils. *Science* 2009;324:1312-4. DOI PubMed
72. Hernandez Y, Nicolosi V, Lotya M, et al. High-yield production of graphene by liquid-phase exfoliation of graphite. *Nat Nanotechnol* 2008;3:563-8. DOI PubMed
73. Edwards RS, Coleman KS. Graphene synthesis: relationship to applications. *Nanoscale* 2013;5:38-51. DOI PubMed
74. Jayasena B, Subbiah S. A novel mechanical cleavage method for synthesizing few-layer graphenes. *Nanoscale Res Lett* 2011;6:95. DOI PubMed PMC
75. Hummers WS, Offeman RE. Preparation of graphitic oxide. *J Am Chem Soc* 1958;80:1339. DOI
76. Marcano DC, Kosynkin DV, Berlin JM, et al. Improved synthesis of graphene oxide. *ACS Nano* 2010;4:4806-14. DOI PubMed
77. Roth WJ, Nachtigall P, Morris RE, Čejka J. Two-dimensional zeolites: current status and perspectives. *Chem Rev* 2014;114:4807-37. DOI PubMed
78. Přech J, Pizarro P, Serrano DP, Čejka J. From 3D to 2D zeolite catalytic materials. *Chem Soc Rev* 2018;47:8263-306. DOI PubMed
79. Hong M, Yu L, Wang Y, et al. Heavy metal adsorption with zeolites: the role of hierarchical pore architecture. *Chemical Engineering Journal* 2019;359:363-72. DOI

80. Li S, Tuan VA, Falconer JL, Noble RD. Separation of 1,3-propanediol from aqueous solutions using pervaporation through an X-type zeolite membrane. *Ind Eng Chem Res* 2001;40:1952-9. DOI
81. Agrawal KV, Topuz B, Jiang Z, et al. Solution-processable exfoliated zeolite nanosheets purified by density gradient centrifugation. *AIChE J* 2013;59:3458-67. DOI
82. Roth WJ, Nachtigall P, Morris RE, et al. A family of zeolites with controlled pore size prepared using a top-down method. *Nat Chem* 2013;5:628-33. DOI PubMed
83. Mazur M, Wheatley PS, Navarro M, et al. Synthesis of 'unfeasible' zeolites. *Nat Chem* 2016;8:58-62. DOI PubMed
84. Lu P, Liu Y, Zhou T, Wang Q, Li Y. Recent advances in layered double hydroxides (LDHs) as two-dimensional membrane materials for gas and liquid separations. *J Membr Sci* 2018;567:89-103. DOI
85. Konch TJ, Dutta T, Neog AB, Gogoi R, Raidongia K. Uphill anion pumping through triangular nanofluidic device of reconstructed layered double hydroxide. *J Phys Chem C* 2021;125:17939-49. DOI
86. Liu J, Yu L, Zhang Y. Fabrication and characterization of positively charged hybrid ultrafiltration and nanofiltration membranes via the in-situ exfoliation of Mg/Al hydrotalcite. *Desalination* 2014;335:78-86. DOI
87. Shao JJ, Raidongia K, Koltonow AR, Huang J. Self-assembled two-dimensional nanofluidic proton channels with high thermal stability. *Nat Commun* 2015;6:7602. DOI PubMed
88. Gogoi RK, Raidongia K. Intercalating cation specific self-repairing of vermiculite nanofluidic membrane. *J Mater Chem A* 2018;6:21990-8. DOI
89. Huang M, Chen Y, Yan X, Guo X, Dong L, Lang W. Two-dimensional Montmorillonite membranes with efficient water filtration. *J Membr Sci* 2020;614:118540. DOI
90. Xiao T, Liu Q, Zhang Q, Liu Z, Zhai J. Temperature and voltage dual-responsive ion transport in bilayer-intercalated layered membranes with 2D nanofluidic channels. *J Phys Chem C* 2017;121:18954-61. DOI
91. Naguib M, Mochalin VN, Barsoum MW, Gogotsi Y. 25th anniversary article: MXenes: a new family of two-dimensional materials. *Adv Mater* 2014;26:992-1005. DOI PubMed
92. Naguib M, Mashtalir O, Carle J, et al. Two-dimensional transition metal carbides. *ACS Nano* 2012;6:1322-31. DOI PubMed
93. Lipatov A, Alhabeb M, Lukatskaya MR, Boson A, Gogotsi Y, Sinitskii A. Effect of synthesis on quality, electronic properties and environmental stability of individual monolayer Ti_3C_2 MXene flakes. *Adv Electron Mater* 2016;2:1600255. DOI
94. Qian HL, Yang CX, Yan XP. Bottom-up synthesis of chiral covalent organic frameworks and their bound capillaries for chiral separation. *Nat Commun* 2016;7:12104. DOI PubMed PMC
95. Pang ZF, Zhou TY, Liang RR, Qi QY, Zhao X. Regulating the topology of 2D covalent organic frameworks by the rational introduction of substituents. *Chem Sci* 2017;8:3866-70. DOI PubMed PMC
96. Wan S, Guo J, Kim J, Ihee H, Jiang D. A belt-shaped, blue luminescent, and semiconducting covalent organic framework. *Angew Chem Int Ed Engl* 2008;47:8826-30. DOI PubMed
97. Shinde DB, Kandambeth S, Pachfule P, Kumar RR, Banerjee R. Bifunctional covalent organic frameworks with two dimensional organocatalytic micropores. *Chem Commun (Camb)* 2015;51:310-3. DOI PubMed
98. Dalapati S, Jin S, Gao J, Xu Y, Nagai A, Jiang D. An azine-linked covalent organic framework. *J Am Chem Soc* 2013;135:17310-3. DOI PubMed
99. Dalapati S, Jin E, Addicoat M, Heine T, Jiang D. Highly emissive covalent organic frameworks. *J Am Chem Soc* 2016;138:5797-800. DOI PubMed
100. Jin S, Sakurai T, Kowalczyk T, et al. Two-dimensional tetrathiafulvalene covalent organic frameworks: towards latticed conductive organic salts. *Chemistry* 2014;20:14608-13. DOI PubMed
101. Dalapati S, Addicoat M, Jin S, et al. Rational design of crystalline supermicroporous covalent organic frameworks with triangular topologies. *Nat Commun* 2015;6:7786. DOI PubMed PMC
102. Jin S, Ding X, Feng X, et al. Charge Dynamics in a donor-acceptor covalent organic framework with periodically ordered bicontinuous heterojunctions. *Angew Chem* 2013;125:2071-5. DOI PubMed
103. Jin S, Furukawa K, Addicoat M, et al. Large pore donor-acceptor covalent organic frameworks. *Chem Sci* 2013;4:4505. DOI
104. Calik M, Auras F, Salonen LM, et al. Extraction of photogenerated electrons and holes from a covalent organic framework integrated heterojunction. *J Am Chem Soc* 2014;136:17802-7. DOI PubMed PMC
105. Chandra S, Kandambeth S, Biswal BP, et al. Chemically stable multilayered covalent organic nanosheets from covalent organic frameworks via mechanical delamination. *J Am Chem Soc* 2013;135:17853-61. DOI PubMed
106. Berlanga I, Ruiz-González ML, González-Calbet JM, Fierro JL, Mas-Ballesté R, Zamora F. Delamination of layered covalent organic frameworks. *Small* 2011;7:1207-11. DOI PubMed
107. Dey K, Pal M, Rout KC, et al. Selective molecular separation by interfacially crystallized covalent organic framework thin films. *J Am Chem Soc* 2017;139:13083-91. DOI PubMed
108. Wang T, Wu H, Zhao S, et al. Interfacial polymerized and pore-variable covalent organic framework composite membrane for dye separation. *Chem Eng J* 2020;384:123347. DOI
109. Zhao M, Yuan K, Wang Y, et al. Metal-organic frameworks as selectivity regulators for hydrogenation reactions. *Nature* 2016;539:76-80. DOI PubMed
110. Hao Z, Wu Y, Zhao Q, et al. Functional separators regulating ion transport enabled by metal-organic frameworks for dendrite-free lithium metal anodes. *Adv Funct Mater* 2021;31:2102938. DOI

111. Gallego A, Hermosa C, Castillo O, et al. Solvent-induced delamination of a multifunctional two dimensional coordination polymer. *Adv Mater* 2013;25:2141-6. DOI PubMed
112. Wang X, Chi C, Zhang K, et al. Reversed thermo-switchable molecular sieving membranes composed of two-dimensional metal-organic nanosheets for gas separation. *Nat Commun* 2017;8:14460. DOI PubMed PMC
113. Peng Y, Li Y, Ban Y, et al. Membranes. Metal-organic framework nanosheets as building blocks for molecular sieving membranes. *Science* 2014;346:1356-9. DOI PubMed
114. Makiura R, Motoyama S, Umemura Y, Yamanaka H, Sakata O, Kitagawa H. Surface nano-architecture of a metal-organic framework. *Nat Mater* 2010;9:565-71. DOI PubMed
115. Acerce M, Voiry D, Chhowalla M. Metallic 1T phase MoS_2 nanosheets as supercapacitor electrode materials. *Nat Nanotechnol* 2015;10:313-8. DOI PubMed
116. Li XL, Li TC, Huang S, Zhang J, Pam ME, Yang HY. Controllable synthesis of two-dimensional molybdenum disulfide (MoS_2) for energy-storage applications. *ChemSusChem* 2020;13:1379-91. DOI PubMed
117. Zhu C, Liu P, Niu B, et al. Metallic two-dimensional MoS_2 composites as high-performance osmotic energy conversion membranes. *J Am Chem Soc* 2021;143:1932-40. DOI PubMed
118. Cheng D, Wang H, Liu B, et al. Dielectric properties and energy-storage performance of two-dimensional molybdenum disulfide nanosheets/polyimide composite films. *J Appl Polym Sci* 2019;136:47991. DOI
119. Hou S, Ji W, Chen J, Teng Y, Wen L, Jiang L. Free-standing covalent organic framework membrane for high-efficiency salinity gradient energy conversion. *Angew Chem* 2021;133:10013-8. DOI PubMed
120. Mijatovic D, Eijkel JC, van den Berg A. Technologies for nanofluidic systems: top-down vs. bottom-up--a review. *Lab Chip* 2005;5:492-500. DOI PubMed
121. Sun P, Zheng F, Zhu M, et al. Realizing synchronous energy harvesting and ion separation with graphene oxide membranes. *Sci Rep* 2014;4:5528. DOI PubMed PMC
122. Cheng H, Zhou Y, Feng Y, et al. Electrokinetic energy conversion in self-assembled 2D nanofluidic channels with Janus nanobuilding blocks. *Adv Mater* 2017;29:1700177. DOI PubMed
123. Hong S, Ming F, Shi Y, et al. Two-dimensional $Ti_3C_2T_x$ MXene membranes as nanofluidic osmotic power generators. *ACS Nano* 2019;13:8917-25. DOI PubMed
124. Wu Y, Xin W, Kong X, et al. Enhanced ion transport by graphene oxide/cellulose nanofibers assembled membranes for high-performance osmotic energy harvesting. *Mater Horiz* 2020;7:2702-9. DOI
125. Zhang Z, Shen W, Lin L, et al. Vertically transported graphene oxide for high-performance osmotic energy conversion. *Adv Sci (Weinh)* 2020;7:2000286. DOI PubMed PMC
126. Liu P, Sun Y, Zhu C, et al. Neutralization reaction assisted chemical-potential-driven ion transport through layered titanium carbides membrane for energy harvesting. *Nano Lett* 2020;20:3593-601. DOI PubMed
127. Xin W, Zhang Z, Huang X, et al. High-performance silk-based hybrid membranes employed for osmotic energy conversion. *Nat Commun* 2019;10:3876. DOI PubMed PMC
128. Zhang Z, Zhang P, Yang S, et al. Oxidation promoted osmotic energy conversion in black phosphorus membranes. *Proc Natl Acad Sci U S A* 2020;117:13959-66. DOI PubMed PMC
129. Li R, Jiang J, Liu Q, Xie Z, Zhai J. Hybrid nanochannel membrane based on polymer/MOF for high-performance salinity gradient power generation. *Nano Energy* 2018;53:643-9. DOI
130. Xiao K, Giusto P, Wen L, Jiang L, Antonietti M. Nanofluidic ion transport and energy conversion through ultrathin free-standing polymeric carbon nitride membranes. *Angew Chem Int Ed Engl* 2018;57:10123-6. DOI PubMed
131. Gao Z, Sun Z, Ahmad M, et al. Increased ion transport and high-efficient osmotic energy conversion through aqueous stable graphitic carbon nitride/cellulose nanofiber composite membrane. *Carbohydr Polym* 2022;280:119023. DOI PubMed
132. Guo W, Cheng C, Wu Y, et al. Bio-inspired two-dimensional nanofluidic generators based on a layered graphene hydrogel membrane. *Adv Mater* 2013;25:6064-8. DOI PubMed
133. Yang G, Lei W, Chen C, et al. Ultrathin $Ti_3C_2T_x$ (MXene) membrane for pressure-driven electrokinetic power generation. *Nano Energy* 2020;75:104954. DOI
134. Qu R, Zeng X, Lin L, et al. Vertically-oriented $Ti_3C_2T_x$ MXene membranes for high performance of electrokinetic energy conversion. *ACS Nano* ;2020:16654-62. DOI PubMed
135. Qin S, Liu D, Chen Y, et al. Nanofluidic electric generators constructed from boron nitride nanosheet membranes. *Nano Energy* 2018;47:368-73. DOI
136. Tollefson J. Power from the oceans: blue energy. *Nature* 2014;508:302-4. DOI PubMed
137. Wang ZL, Jiang T, Xu L. Toward the blue energy dream by triboelectric nanogenerator networks. *Nano Energy* 2017;39:9-23. DOI
138. Jie Y, Jia X, Zou J, et al. Natural leaf made triboelectric nanogenerator for harvesting environmental mechanical energy. *Adv Energy Mater* 2018;8:1703133. DOI
139. Lin ZH, Cheng G, Lin L, Lee S, Wang ZL. Water-solid surface contact electrification and its use for harvesting liquid-wave energy. *Angew Chem Int Ed Engl* 2013;52:12545-9. DOI PubMed
140. Wen X, Yang W, Jing Q, Wang ZL. Harvesting broadband kinetic impact energy from mechanical triggering/vibration and water waves. *ACS Nano* 2014;8:7405-12. DOI PubMed
141. Zhao Y, Wang J, Kong XY, et al. Corrigendum to Robust sulfonated poly (ether ether ketone) nanochannels for high-performance

osmotic energy conversion. *Natl Sci Rev* 2020;7:1793. DOI PubMed PMC

142. Hou S, Zhang Q, Zhang Z, et al. Charged porous asymmetric membrane for enhancing salinity gradient energy conversion. *Nano Energy* 2021;79:105509. DOI